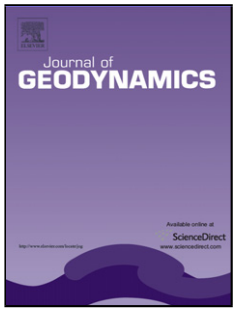

Autochtonous origin of the Encruzilhada Block, Dom Feliciano Belt, southern Brazil, based on aerogeophysics, image analysis and PT-paths

Giuseppe Betino De Toni (Conceptualization) (Methodology) (Formal analysis) (Investigation) (Writing - original draft), Maria de Fátima Bitencourt (Supervision) (Writing - review and editing) (Project administration) (Funding acquisition), Jiří Konopásek (Supervision) (Validation) (Writing - review and editing) (Project administration) (Funding acquisition), Matheus Ariel Battisti (Investigation), Elisa Oliveira da Costa (Validation), Jairo Francisco Savian (Data curation) (Validation) (Resources)

PII: S0264-3707(21)00011-9

DOI: https://doi.org/10.1016/j.jog.2021.101825

Reference: GEOD 101825

To appear in: *Journal of Geodynamics*

Received Date: 6 September 2020

Revised Date: 11 January 2021

Accepted Date: 1 February 2021

Please cite this article as: De Toni GB, de Fátima Bitencourt M, Konopásek J, Battisti MA, da Costa EO, Savian JF, Autochtonous origin of the Encruzilhada Block, Dom Feliciano Belt, southern Brazil, based on aerogeophysics, image analysis and PT-paths, *Journal of Geodynamics* (2021), doi: https://doi.org/10.1016/j.jog.2021.101825

Autochtonous origin of the Encruzilhada Block, Dom Feliciano Belt, southern Brazil, based on aerogeophysics, image analysis and PT-paths

Giuseppe Betino De Toni[1,2]*, Maria de Fátima Bitencourt[1], Jiří Konopásek[3,4], Matheus Ariel Battisti[1], Elisa Oliveira da Costa[1], Jairo Francisco Savian[1]

[1] Programa de Pós-graduação em Geociências, Instituto de Geociências, Universidade Federal do Rio Grande do Sul, Av. Bento Gonçalves, 9500, Porto Alegre, 91500-000, RS, Brazil.

[2] Present address: Polytechnic School, Universidade do Vale do Rio dos Sinos (UNISINOS), Av. Unisinos, 950, São Leopoldo, 93022-750, RS, Brazil

[3] Department of Geosciences, UiT The Arctic University of Norway, Postboks 6050 Langnes, 9037 Tromsø, Norway. E-mail: jiri.konopasek@uit.no

[4] Czech Geological Survey, Klárov 3, 118 21, Prague, Czech Republic

*Corresponding author: detoni.geo@gmail.com, giuseppebt@unisinos.br

Graphical abstract

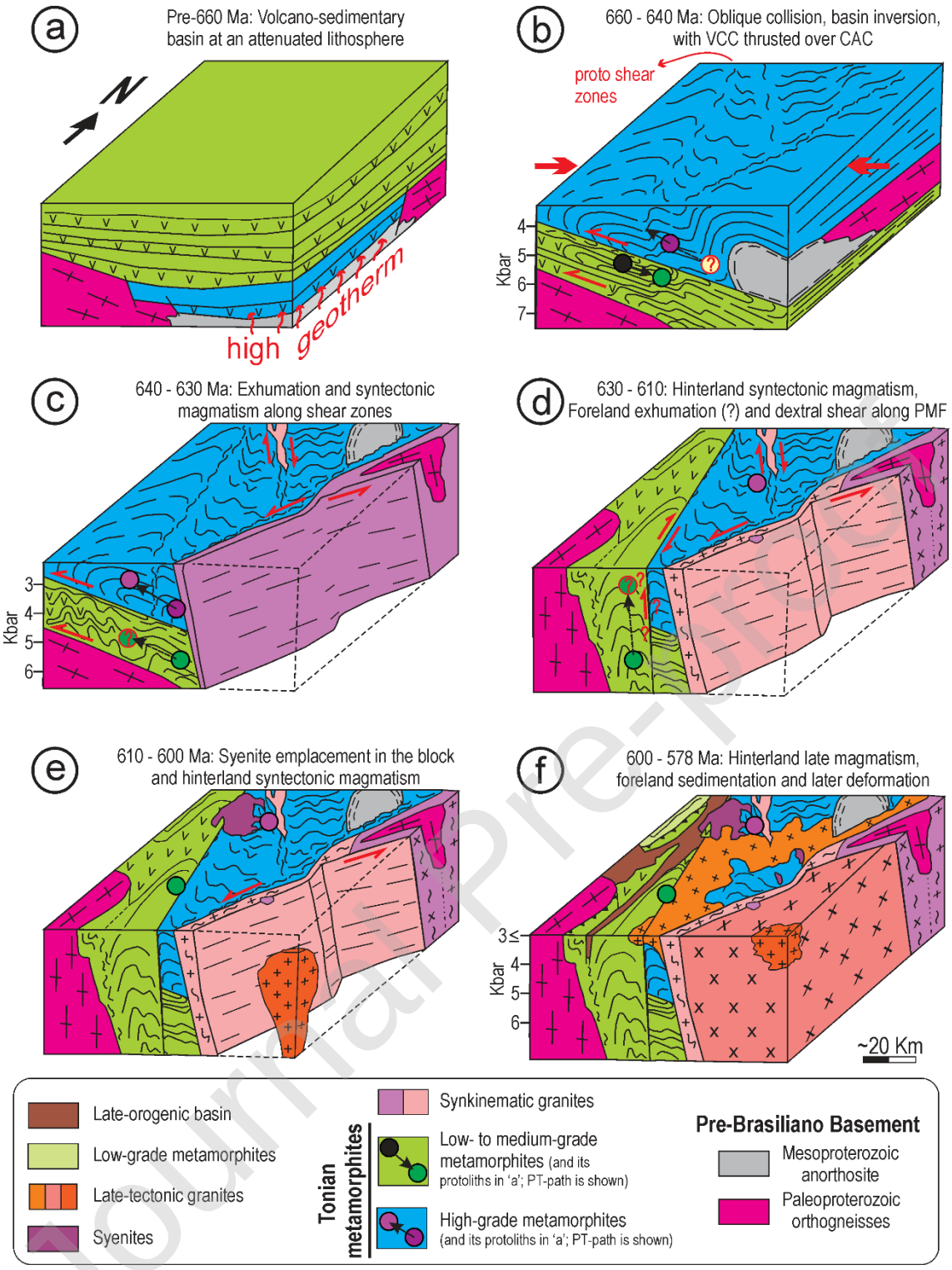

ABSTRACT

The Encruzilhada Block lies between the eastern hinterland and western foreland of the Dom Feliciano Belt (southern Brazil) and its tectonic meaning in the orogenic evolution of the belt is still poorly understood. Its low magnetic signal is similar to that of the foreland supracrustal sequences, whereas the high gammaspectrometric signal appears due to the hinterland post-collisional

granitoids. Satellite image lineament analysis points to tectonic similarities between the Encruzilhada Block and the foreland, as the structures in both domains show predominantly NNW and NNE trends, while the hinterland mostly presents NE-trending structures. The pre-orogenic connection between the Encruzilhada Block and the foreland is indicated by the correlation between the Várzea do Capivarita and Cerro da Árvore complexes. Both contain 800 – 780 Ma metaigneous rocks with arc-like geochemistry, and parametamorphic rocks with similar sedimentary provenance. Common syn-orogenic deformation history of both complexes is suggested by progressive top-to-the-W transpressive deformation and similar peak metamorphic age (660 – 640 Ma). PT-paths suggest exhumation of the hinterland Várzea do Capivarita Complex from high-T/low-P conditions of 790 – 820 °C/4.4 – 4.8 kbar to 660 – 720 °C/2.5 – 3.4 kbar at ca. 630 Ma. On the other hand, the foreland Cerro da Árvore Complex was subject to progressive metamorphism from 555 – 565 °C/5.4 – 5.7 kbar to 560 – 580 °C/5.8 – 6.3 kbar, which is interpreted as a result of orogenic thickening. Evidence suggests that both complexes have originated in a similar, if not a single, basin on an attenuated lithosphere with high geothermal gradient, possibly a (back-arc?) rift. Oblique collision has caused basin inversion and thrusting of the lower crust over the rift margin, which may have been accompanied by lithosphere delamination. Progressive transpressional deformation and voluminous post-collisional magmatism (640 – 578 Ma) controlled by major lineaments have blurred the original tectonic contact and finally caused thermal metamorphism in both complexes at ca. 3 kbar, when the autochtonous Encruzilhada Block was stabilized in its present geological configuration. The intracontinental character of major shear zones requires a review of the existing evolutionary model for the Dom Feliciano Belt hinterland in the context of Western Gondwana amalgamation.

Keywords: Aeromagnetometry, Aerogammaspectrometry; Pseudosection; High-T/Low-P; intracontinental shear zone

1. Introduction

Distinguishing the native or exotic character of crustal blocks is essential to understand the geological evolution of orogenic belts, and this should be done

based on multiple and independent criteria (e.g. Sengör and Dewey, 1990; Burton-Johnson and Riley, 2015). The pre-orogenic position of various crustal blocks is a central question in recent models for the Western Gondwana amalgamation (Fig. 1a), in which the major tectonic boundaries of the Mantiqueira Province (Almeida et al., 2000) mobile belts are interpreted either as sutures (e.g. Chemale Jr., 2000; Basei et al., 2005, 2008; Passarelli et al., 2011; Heilbron et al., 2020) or intracontinental shear zones (e.g. Florisbal et al., 2012; Oriolo et al., 2016a, 2017; Konopásek et al., 2018; Meira et al., 2015, 2019; Fossen et al., 2020; De Toni et al., 2020a, b; Percival et al., 2021).

The presence of high-T/low-P granulites in the Mantiqueira Province is conspicuous (e.g. Gross et al., 2006; 2009; Meira et al., 2019; Costa et al., 2020), and their tectonic setting is still a matter of debate. As pointed out by Kelsey and Hand (2011), high-T/low-P conditions are not expected for an overthickened lithosphere. Collision and tickening of a previously extended crust is assumed to account for the combination of high geothermal gradients and gently dipping contractional structures (Harris and Holland, 1984; Thompson et al., 2001; Clark et al., 2011; Fowler et al., 2015). A sequence of tectonic pull and push is expected when collision follows the opening of a rift or back-arc rift (Lister and Foster, 2009; Fowler et al., 2015). Recent models for the Musgrave Orogeny (central Australia) by Gorczyk and Vogt (2015) suggest that lithospheric delamination occured during contraction of previously weakened domains limited by cratonic blocks in an intracontinental setting, causing anomalously high geothermal heat flux distant from active plate boundaries.

In this study we investigate a “suspect terrane” of the Neoproterozoic Dom Feliciano Belt, southernmost Brazil. The Encruzilhada Block (as defined by Jost and Hartmann, 1984) is distinguished from the rest of the belt by its rock association, including the high-T/low-P Várzea do Capivarita Complex (VCC – e.g. Gross et al., 2006; Costa et al., 2020), abundant syenites and an anorthosite body. The block is separated from the hinterland Pelotas Batholith by the large-scale Dorsal de Canguçu Shear Zone, and from the foreland Tijucas Fold Belt by the Passo do Marinheiro Fault (Fig. 1b). The tectonic significance of the Encruzilhada Block remains poorly understood. Apart from its position between the orogenic hinterland and foreland, the block presents

geophysical characteristics compatible with both domains (Hartmann et al., 2016). Large-scale aeromagnetometry and aerogammaspectrometry data together with structural data of the Encruzilhada Block are integrated with PT data from the high-T/low-P (cordierite+spinel)-bearing metapelite of Várzea do Capivarita Complex and a medium-grade schist of the easternmost foreland. Finally, we discuss the origin of the block and its role in the Dom Feliciano Belt tectonic evolution.

2. Geological Setting

2.1 Regional Geology

The Precambrian geology of southern Brazil and Uruguay is represented by two main cratonic blocks - the Luis Alves Craton (Hartmann et al., 2000) in the north and the Rio de la Plata Craton + the Nico Perez Terrane (Oyhantçabal et al., 2011) in the south - and the Dom Feliciano Belt along their eastern margin (Fig. 1a).The belt is the South American portion of the Dom Feliciano-Kaoko-Gariep orogenic system, formed during the Western Gondwana assembly (Oriolo et al., 2017; Konopásek et al., 2018).

The Dom Feliciano Belt comprises three main tectonic domains limited by major lineaments (Fernandes et al., 1995a, 1995b; Hartmann et al., 2016) (Fig. 1b). The western São Gabriel Block, exposed exclusively in southernmost Brazil, represents a juvenile, early-Neoproterozoic magmatic arc (Babinski et al., 1996) with remnants of *ca.* 930 to 900 Ma oceanic crust, ca. 890 and 860 Ma fragmentary arc record, ca. 790 ophiolite accretion and a well-preserved continental magmatic arc active from *ca.* 770 to 720 Ma (Arena et al., 2016; Philipp et al., 2018). East of the São Gabriel Block, two ca. 1200 km long domains represent the foreland and hinterland domains, which extend from southern Brazil to Uruguay (Fig. 1b).

The foreland Tijucas Fold Belt (Hasui et al., 1975) is a deformed and metamorphosed multi-phase, volcano-sedimentary basin (e.g. Gruber et al., 2016a; Pertille et al., 2015; Höfig et al., 2017). In southernmost Brazil it is composed of two distinct sequences tectonically imbricated due to a westward-vergent thrust (Jost and Bitencourt, 1980; Höfig et al., 2017; Battisti et al., 2018). Volcanic activity in this basin was dated at ca. 780 Ma (Saalmann et al., 2011; Martil, 2016) and between ca. 600 and 580 Ma (Höfig et al., 2017).

Recurrent, collision-related metamorphic/deformational events took place at *ca.* 650 Ma (Lenz, 2006) and shortly after 570 Ma (Höfig et al., 2017; Battisti et al., 2018), giving rise to a sequence of regional antiformal structures (Fig. 2a). According to Jost and Bitencourt (1980), the Cerro da Árvore Complex (CAC – Porongos I *sensu* Höfig et al., 2017; Battisti et al., 2018) was thrust over the Cerro dos Madeiras Group (Porongos II *sensu* Höfig et al., 2017; Battisti et al., 2018). The Cerro da Árvore Complex features tectonic interleaving of metapelites and metavolcanic rocks with increasing metamorphic grade from west to east (Jost and Bitencourt, 1980; Jost, 1981; Lenz, 2006). Paleoproterozoic basement inliers outcrop in the core of some regional antiforms (e.g. Encantadas Complex – Saalmann et al., 2006), whilst non-metamorphosed Ediacaran to Cambrian volcano-sedimentary successions fill NS-trending narrow grabens between the antiforms (Borba et al 2007; Paim et al 2014; de Oliveira et al, 2014; Fambrini et al., 2018).

Figure 1

Farther east, along the orogenic hinterland, granitic rocks that form the Pelotas Batholith and its extension towards the north and south (Fig. 1b) are interpreted as resulting from post-collisional magmatism. These granites were formed between *ca.* 640 and 580 Ma and the magmatic pulses were controlled by an anastomosing array of shear zones known as the Southern Brazilian Shear Belt that acted as channels for both crustal and mantle-derived magmas (Bitencourt and Nardi, 2000; Philipp et al., 2002, 2005). Recent studies suggest that this transpressive shear belt affected both the hinterland batholiths and the supracrustals of the Tijucas Fold Belt (Oriolo et al., 2016a; Battisti et al., 2018; De Toni et al., 2020b).

Paleoproterozoic TTG gneisses (Gregory et al., 2015, 2017) are found as roof pendants in the granitoids between the Dorsal do Canguçu (Picada, 1971; Fernandes and Koester, 1999; Vieira et al., 2020) and Quitéria-Serra do Erval shear zones (Gregory et al., 2015, 2017) (Fig. 2a). Two roof pendants are reported in the post-collisional granites of the Encruzilhada Block (Fig. 2a). The northern roof pendant features the Mesoproterozoic Capivarita Anorthosite (Chemale Jr. et al, 2011) surrounded by ortho- and paragneisses of the Várzea

do Capivarita Complex. The southern roof pendant contains Várzea do Capivarita Complex gneisses (Gross et al., 2006; Bom et al., 2014; Philipp et al., 2016; Martil et al., 2011, 2017; Martil, 2016; Costa et al., 2020). Additionally, km-sized blocks and xenoliths of orthogneisses are found throughout the hinterland batholiths (e.g. Silva et al., 1999; Koester et al., 2016; Tambara et al., 2019; De Toni et al., 2020a) (Fig. 1b). Based on the similar protolith ages and geochemical signatures, these early Neoproterozoic gneisses were correlated with gneisses of the Punta del Este Terrane in Uruguay exposed in the southeast portion of the Dom Feliciano Belt (Oyhantçabal et al., 2009; Lenz et al., 2011; 2013; Masquelin et al., 2012; Ramos et al., 2018) (Fig. 1b).

The 800 – 780 Ma calc-alkaline, arc-like metavolcanic rocks of the Cerro da Árvore Complex were correlated with the Várzea do Capivarita Complex orthogneisses and coeval units from southern Brazil and Uruguay. Their similarity serves as an additional evidence that the hinterland and foreland of the Dom Feliciano Belt have been part of the same orogenic system since pre-collisional times (Martil et al., 2017; Battisti et al., 2018; De Toni et al., 2020a). Such interpretation questions accretionary models (e.g. Basei et al., 2005, 2008; Chemale Jr., 2000). An alternative interpretation of the Dom Feliciano Belt tectonic setting was published by Konopasek et al. (2018), whereby the Várzea do Capivarita Complex and correlated units are considered as deep crustal counterparts of rift-related volcano-sedimentary sequences recognized in the Kaoko Belt. Based on petrological evidence and tectonic correlation across the main tectonic domains of the Dom Feliciano Belt, De Toni et al. (2020a) suggested that these rocks formed as arc-related magmatism within ca. 800 –- 770 Ma period of eastward flat-slab subduction that promoted migration of arc magmatism towards the continent, away from the São Gabriel Block.

2.2 Geology of the Encruzilhada Block

The Encruzilhada Block (Fig. 2a) is considered to be the northwestern portion of the Pelotas Batholith (e.g. Jost and Hartmann, 1984; Philipp and Machado, 2002, 2005; Hartmann et al., 2016). It was originally defined because of peculiar rock association absent in the neigbouring blocks. Apart from the granulite-facies rocks of the Várzea do Capivarita Complex (Costa et al., 2020), it contains the Mesoproterozoic Capivarita Anorthosite (Chemale Jr. et al., 2011)

and a sequence of syn- to post-collisional syenite intrusions with ages from 640 to 578 Ma (Bitencourt et al., 2016; Nardi et al., 2008; Rivera, 2019; Padilha et al., 2019).

Figure 2

The limit between the Encruzilhada Block and the Pelotas Batholith is the sinistral transcurrent Dorsal de Canguçu Shear Zone, where post-collisional, syntectonic, high-K calc-alkaline and peraluminous granites were emplaced between ca. 635 and 605 Ma (Fernandes and Koester, 1999; Vieira et al., 2020). The boundary between the block and the Tijucas Fold Belt is the Passo do Marinheiro Fault (Picada, 1971; Fig. 2a). This fault was interpreted by Jost (1981) as an originally dextral ductile structure marked by the Cerro da Árvore Complex regional-scale drag fold (Fig. 2a). On the other hand, the Passo do Marinheiro Fault is usually interpreted as a sinistral, brittle structure, due to apparent displacement of the southwestern portion of the Encruzilhada Granite (e.g. Picada, 1971, Jacobs et al., 2018) (Fig. 2a).

2.2.1 Várzea do Capivarita Complex

The Várzea do Capivarita Complex comprises igneous and metamorphic rocks of the Encruzilhada Block (Fig. 2a). Characteristic rock types are high-temperature, tectonically interleaved tonalitic–granitic orthogneisses with Tonian protolith, and paragneisses including metapelites, calc-silicate rocks, marbles and rare quartzites (Gross et al., 2006; Martil et al., 2011, 2017; Martil, 2016; Gruber *et al.*, 2016b; Costa et al., 2020).

In the eastern portion of the northern roof pendant, Várzea do Capivarita Complex gneisses surround the Capivarita Anorthosite present in the core of a regional antiform (Fig. 2a). Both rock associations were metamorphosed and deformed under granulite facies conditions at *ca.* 650 – 640 Ma (Chemale Jr., 2011; Martil, 2016; Martil et al., 2017), contemporaneous to the intrusion of the Arroio das Palmas Syenite (De Toni et al., 2016; Bitencourt et al., 2016).

The structural characterization of the progressive transpressional deformation of the Várzea do Capivarita Complex gneisses was presented by Martil (2016) and Martil et al. (2017). The complex records an early foliation (S_1 – Fig. 2b) which

strikes about 340° and dips at shallow angles to the east. A highly oblique stretching lineation (L_1) lies in the S_1 foliation plane, and its top-to-the-W kinematics is registered by outcrop-scale asymmetric folds, asymmetric porphyroclasts, and S-C fabrics. The verticalization of S_1 towards the fold short limbs was accompanied by the rotation of the lineation L_1 towards subhorizontal position within dextral strike-slip domains (S_2, L_2 – Fig. 2c). D_1 and D_2 were progressive under granulite-facies conditions. This progression is recorded by orthopyroxene in tonalitic orthogneisses stable in both fabrics, wich show similar age for the granulite-facies metamorphism (Martil et al., 2011, 2017; Martil, 2016). Syenite syntectonic emplacement occurred along both fabrics (De Toni et al., 2016; Bitencourt et al., 2016). A D_2 high-strain zone was recognized at the western portion of the northern roof pendant (Martil, 2016; Martil et al., 2017; De Toni et al., 2016; Lyra et al., 2018). The zone is named here the Passo das Canas Shear Zone (Fig. 2a) and it controlled syntectonic intrusions such as the Arroio das Palmas Syenite (De Toni et al., 2016) and the sillimanite-bearing Butiá Granite (Niessing, 2008; Lyra et al., 2018).

The Várzea do Capivarita Complex high-T/low-P metamorphic conditions were estimated by Gross et al. (2006) in the range of 730 – 800°C and 3 to 4 kbar. In contrast, Bom et al. (2014) and Philipp et al. (2013, 2016) argued for medium-P/high-T conditions. Costa et al. (2020) modelled the PT paths of metapelitic gneisses of the southern roof pendant, and described abundant partial melting features. Estimated peak metamorphic conditions at ca. 800°C/4.6 kbar reinforced and refined the estimates of Gross et al. (2006). Costa et al. (2020) also presented evidence of rapid exhumation to shallow conditions at ca. 680°C/2.8 kbar, facilitated by significant volume of melt under high geothermal gradient.

Martil (2016) reported protolith ages of 790-770 Ma for the orthogneisses, and high-grade metamorphism between 650-640 Ma (U-Pb zircon LA-ICP-MS and SHRIMP). A collision-related metamorphic age of 651.5 ± 8.8 Ma (U-Pb titanite LA-ICP-MS) for the Capivarita Anorthosite was reported by Chemale Jr. et al. (2011). On the other hand, Gross et al. (2006) reported a 626–604 Ma metamorphic age for the Várzea do Capivarita Complex metapelitic granulites (Sm-Nd garnet and whole-rock two-point isochron). Similar ages of 620 ± 6.3 and 619 ± 4.3 Ma (U-Pb zircon SHRIMP) were reported by Philipp et al. (2016)

from a leucogranite vein and migmatitic metapelite, respectively. These ages are interpreted to result from synchronous migmatitization and leucosome crystallization after the metamorphic peak, as exemplified by Himalayan anatexis, which occurred 30 Ma after the main collisional episode (Weinberg, 2016).

Despite the diferences in estimated timing and PT conditions of the high-grade metamorphism reported by different authors, the granulite-facies deformational fabric of the Várzea do Capivarita Complex is considerd as an evidence for a collisional episode in the central part of the Dom Feliciano Belt (Gross et al., 2006; Philipp et al., 2013, 2016; Martil, 2016; Martil et al., 2011, 2017; Costa et al., 2020).

2.2.2 Encruzilhada Block intrusive rocks

The Encruzilhada Block was intruded by several granite and syenite units. The sillimanite-bearing Butiá Granite (Niessing, 2008; Lyra et al., 2018) crystallized at 629.2 ± 6.8 Ma (U-Pb monazite ID-TIMS – Bitencourt et al., 2015) and is syntectonic to the dextral strike-slip Passo das Canas Shear Zone (Fig. 2a). The emplacement conditions were determined at 700 – 750 °C and 3.0 – 4.2 kbar based on microstructural analysis and mineral chemistry (Niessing, 2008). The Butiá Granite was correlated with other small peraluminous leucogranitic intrusions related to partial melting of the VCC rocks (Bom et al., 2014; Philipp et al., 2016; Costa et al., 2020) and syntectonic granites of similar age of the Pelotas Batholith emplaced along shear zones, such as the Cordilheira Suite intruding the Dorsal de Canguçu Shear Zone (Philipp et al., 2013; Lyra et al., 2018; Vieira et al., 2020).

The Piquiri Syenite Massif is a landmark in the Encruzilhada Block due to its unambiguous horse-shoe shape in map view, kilometer-size (10 – 15 km in diameter) and pronounced positive relief. This intrusion crosscuts the Passo do Marinheiro Fault considered to be the western limit of the block (Fig. 2a). The Piquiri Syenite Massif is an ultrapotassic-shoshonitic association of syenites, granites and lamprophyres (Stabel et al., 2001; Nardi et al., 2008), which built the massif in pulses (Sbaraini et al., 2020) from 609 ± 2 Ma to 584 ± 2 Ma (Rivera, 2019). The Piquiri Syenite Massif emplacement caused localized contact metamorphism of Várzea do Capivarita Complex xenoliths and meter-

scale roof pendants, and erased the foliation of the Cerro da Árvore Complex metavolcanic roof pendant (Martil, 2007; Battisti et al. 2018). From these observations we conclude that the syenite was emplaced after the Várzea do Capivarita and Cerro da Árvore complexes were positioned side-by-side. Other syenitic intrusions of similar age, such as the Arroio do Silva Pluton (578 ± 4 Ma – LA-ICP-MS U-Pb zircon - Padilha et al., 2019) occur in the southern roof pendant (Fig. 2) and similarly caused contact metamorphism in metapelitic paragneisses.

The Encruzilhada Granite (Fig. 2) is the youngest intrusion in the Encruzilhada Block, containing xenoliths of the Arroio do Silva Pluton syenites (Padilha et al., 2019). This A-type granite is coeval with mafic magma of tholeiitic affinity (Jacobs et al., 2018). Contact metamorphism on the Cerro da Árvore Complex metapelites west of Passo do Marinheiro Fault was attributed by Lenz (2006) to the emplacement of the Encruzilhada Granite .

3. Materials and methods

An integrated map of the Encruzilhada Block and surroundings is presented (Fig. 2a), compiled from the mapping program led by Universidade Federal do Rio Grande do Sul (UFRGS, 2008, 2009, 2010, 2011). Geophysical data result from airborne magnetic and gamma-ray spectrometric survey done by the Geological Survey of Brazil (CPRM, 2010) in southernmost Brazil, with line spacing of 500 m and control lines spaced of 10,000 m (N-S and E-W). Geophysical data was processed with processed with Oasis Montaj (GEOSOFT, 2005).Two adjacent ASTER images were processed by combination of visible and near-infrared (VNIR) band 3 nadir and backwards to build 3D anaglyphs and a digital elevation model of the area with ERDAS Imagine (2014). Lineament tracing at regional scale (1:200.000 scale) resulted in 391 line segments displayed in frequency rose diagrams.

Metamorphic conditions were estimated from two representative metapelitic samples: a spinel-cordierite-garnet-biotite gneiss of the Encruzilhada Block (Várzea do Capivarita Complex, sample MN-12C) and a garnet-staurolite-quartz-mica schist from the easternmost foreland (Cerro da Árvore Complex, sample MAB-52A). Modelling was done with the Perple_X 6.7.0 software (Connoly, 2005) and the thermodynamic database of Holland and Powell (1998,

revised 2004). We used the mixing models for feldspar (Fuhrman and Linsdley, 1988), pyroxene (Holland and Powell, 1996), muscovite (Coggon and Holland, 2002), biotite (Tajčmanová et al., 2009), chlorite (Holland et al., 1998) and melt (Holland and Powell, 2001; White et al., 2001). Pseudosections were constructed from bulk chemistry of major elements, whilst mineral chemical data were used for refinement of the PT estimates. Whole-rock compositions were obtained from rock powder tablets in representative samples using a Rigaku RIX 2000 X-Ray Fluorescence, in the X-ray Fluorescence Laboratory from Centro de Estudos em Petrologia e Geoquímica (CPGq), Instituto de Geociências, Universidade Federal do Rio Grande do Sul (UFRGS), Brazil (methods detailed in Brown et al., 1973). Microscopic-scale subdomains recognized in one sample (MN-12C) were assumed to be closed systems, and their composition was obtained by compositional mapping using a Scanning Electron Microscope (SEM) Zeiss Merlin VP Compact from the SEM Laboratory of the Health Sciences Faculty, UiT The Arctic University of Norway in Tromsø. The approach followed the method described in Tajčmanová et al. (2007). Thin sections were carbon-coated and analytical conditions were 20 kV acceleration voltage and 120 µm aperture. Mineral compositions were determined at the Microprobe Laboratory, CPGq, UFRGS, using a Cameca SXFive microprobe at analytical conditions of 14.8 keV, 15 nA current, and beam size of 20 µm.

4. Remote sensing and aerogeophysical characteristics of the Encruzilhada Block

4.1 Satellite image analysis and tectonic framework

Tracing of 391 lineaments over the DEM is presented in terms of a lineament map (Fig. 3a) and frequency rose diagrams for the whole dataset (Fig. 3b) and for each considered domain (Fig. 3c to e). The domain limits are the geological boundaries of the Encruzilhada Block, i.e. the Passo do Marinheiro Fault and the Dorsal de Canguçu Shear Zone.

The most frequent lineaments strike approximately north-south. The general diagram presents two maxima (22 lineaments each) at 350-360° and 010-020°, and additional secondary concentrations between 340° and 030°. Rose diagrams for each domain show similar patterns. The Encruzilhada Block domain (Fig. 3c) presents maximum lineament concentration at 340°-350°, with

secondary maxima at 000-010° and 020-030°. NW-striking lineaments are present and NE-striking lineaments are rare. On the other hand, the Pelotas Batholith domain (Fig. 3d) presents a maximum at 050-060° and two secondary concentrations at 040-050° and 080-090°. There is a minor occurrence of NNW and NNE directions, while NW-striking lineaments are virtually absent. In the Tijucas Fold Belt domain (Fig. 3e), only two maxima are found at 350-360° and 010-020°, and both NE- and NW-striking lineaments are rare.

The Encruzilhada Block lineament pattern is therefore similar to that of the Tijucas Fold Belt, possibly related to a common structural evolution, as already mentioned by Battisti et al. (2018) and also apparent from the stereoplots (Fig. 2b, c and d). On the other hand, such pattern is in contrast with that of the Pelotas Batholith domain, clearly controlled by the Dorsal de Canguçu Shear Zone, which points to a different origin or an important structural overprint.

Figure 3

4.2 Aerogeophysical signatures

The aeromagnetometric analytical signal amplitude of the total magnetic field (Fig. 4a), aerogammaspectrometry total counts (Fig. 4b) and ternary composition (Fig. 4c) maps covering the Encruzilhada Block (same area as Fig. 2a) are presented in Figure 4. A sketch for the three geophysical maps is presented in Figure 4d.

Figure 4

The aeromagnetometric map (Fig. 4a) shows contrasting patterns for the Encruzilhada Block relative to neighbouring areas. The map is divided into three magnetic domains (Md), each one further subdivided into two subdomains due to internal heterogeneity, and named from west to east, Md1a, Md1b, Md2a, Md2b, Md3a and Md3b (Fig. 4d). The block shows a dominantly low magnetic signal (center of Fig. 4a; Md2a in Fig. 4d). According to Shroder (2014), sedimentary rocks are less magnetic than igneous rocks, and negative magnetic anomalies are typical of sedimentary basins or troughs. The low signal of the block is probably due to the pronounced thickness of

metasedimentary rocks as the main source of the negative anomaly, with no significant magnetic bodies in depth. Higher isolated aeromagnetic signals in the Encruzilhada Block are related to the Piquiri Syenite Massif (nearly circular, positive anomaly in Fig. 4a; Md2b in Fig. 4d) and other syenitic intrusions (smaller patches with positive anomaly at the center of Figure 4a).

The foreland Tijucas Fold Belt is characterized by dominantly medium (Md1a) magnetic signal, with a NNE-trending elongate, highly magnetic body in the northern part (Md1b). This feature is attributed to a portion of the Capané Antiform, where a mafic-ultramafic sequence was described (Marques et al., 2003). The contact between Md1a and Md2a is marked by an abrupt boundary between dominantly medium and low magnetic signals, and mostly coincides with the Passo do Marinheiro Fault.

The limit between Md2 and Md3 is given by a well-marked discontinuity separating the low-signal Md2a and the dominantly high signal eastern portion. This structure is named the Porto Alegre Lineament (after Fernandes et al., 1995b – PAL in Fig. 4d), and coincides with the southern boundary of the Quitéria-Serra do Erval Shear Zone (Gregory et al., 2015, 2017) in the northern part of the study area. The Porto Alegre Lineament also merges with the Dorsal de Canguçu Shear Zone towards the south (Fernandes et al., 1995b). The third magnetic domain is subdivided into a northern, medium-signal domain (Md3a) and a southern, high-signal domain (Md3b). The limit between subdomains is an irregular boundary, probably related to intrusive contacts of distinct granitoids.

Several high-signal lineaments are oriented E-W to WNW-ESE and are observed mainly in the southern half of the map. These lineaments crosscut all magnetic domains and structures described, and are interpreted by Hartmann et al. (2016) to represent Mesozoic dikes.

The aerogammaspectrometric total count map (Fig. 4b) shows the difference between the foreland Tijucas Fold Belt with low count values in the western portion (Gd1a and Gd1b), and the Encruzilhada Block dominantly higher count values (Gd2a and Gd2b). The block is in sharp contact with the Dorsal de Canguçu Shear Zone (Gd3) and the rest of the Pelotas Batholith (Gd4). The higher values within the block, apart from the Piquiri Syenite Massif (Fig. 2 and 4b), are mostly equivalent to the Encruzilhada Granite. The low count spot at

the upper-center of Figure 4b is the Capivarita Anorthosite (Gd2c in Fig. 4d). The surrounding area, with relatively low count values, is the Várzea do Capivarita Complex northern roof pendant. Similar low counts are also found in the Cerro da Árvore Complex (greenish Gd1b). The medium-to-high values of the southern roof pendant may indicate pervasive Encruzilhada Granite injections in the country rocks (Jacobs et al., 2018) and/or relatively higher proportion of partial melting described in metapelites of the Várzea do Capivarita Complex when compared to the northern roof pendant (Costa et al., 2020).

The contact between the Encruzilhada Block and Pelotas Batholith is marked by mylonites and syntectonic granites along the Dorsal de Canguçu Shear Zone (Gd3 in Fig. 4d). It is a relatively low-count, NE-striking, narrow and elongate area which widens in its northern portion and splits into the ENE-striking Quiteria-Serra do Erval Shear Zone to the east (Fig. 4b). In the remaining part of the batholith different shades of hot colours are found. Among them, several NNE- to NE-trending structures of sigmoidal pattern are observed, especially in the lower half of the Pelotas Batholith (Fig. 4b and 4d).

The aerogammaspectrometric ternary representation (Fig. 4c) shows the difference between the foreland Tijucas Fold Belt, with low count values (darker) in the western portion, and the Encruzilhada Block and Pelotas Batholith higher count values (dominantly light colours). These subdivisions are more diffuse than in other maps, but are in agreement with the observed contact between Md3a and Md3b in the aeromagnetometric map (Fig. 4a and 4d). Again, several NNE-trending structures are observed along the Pelotas Batholith which drag the NE-trending main structures with apparent sinistral shear sense.

A black spot marks the Capivarita Anorthosite at the northeastern portion of the Encruzilhada Block, surrounded by bluish/greenish high-grade gneisses of the Várzea do Capivarita Complex. A light pink spot marks the Piquiri Syenite Massif in the northwestern corner of the block. On the western side of the block, gneisses occur in the dominantly bluish area, where the northern and southern roof pendants contrast with the brighter areas of younger magmatic rocks which have obliterated possible contacts between the high-grade rocks of the block and the lower-grade metamorphites westwards.

West of the Passo do Marinheiro Fault, the foreland Tijucas Fold Belt may be subdivided into three domains of different aerogammaspetrometric response: (i) a dominantly reddish-brown domain to the northwest (Gd1a), with delicate, N30E-striking, reddish and purplish lineaments which represent the Piquiri Basin (Borba et al., 2007; Fambrini et al., 2018) and the Capané Antiform (Marques et al., 2003; Höfig et al., 2017), respectively; (ii) the Cerro da Árvore Complex, of dominantly purple colour (Gd1b); and (iii) the slightly lighter red in the southwestern portion of the map, which is the Encantadas Complex (Gd1c - Fig. 4d). The northwestern, dark-blue portion of the map, as well as the extreme southeastern black portion, are younger sedimentary cover.

5. PT estimates

Comparison of PT-paths of the Várzea do Capivarita and Cerro da Árvore complexes aims at bringing information about the relative position and trajectories of the Encruzilhada Block and Tijucas Fold Belt during metamorphism, as their syn-tectonic contact relationship was blurred by late-tectonic intrusions.

5.1 Sample description and mineral chemistry

Two metapelitic rocks, one from each complex, were studied for comparison: a weakly migmatitic spinel-cordierite-garnet-biotite paragneiss (sample MN-12C) collected from the Várzea do Capivarita Complex, located in the northern roof pendant of the Encruzilhada Block and a staurolite-garnet mica schist (MAB-52A) from the Cerro da Árvore Complex, collected in the neighbouring foreland Tijucas Fold Belt. Contact metamorphism locally recorded in the schist (Lenz, 2006) was also observed in a second sample of the Cerro da Árvore Complex collected from the same outcrop. Sample locations are presented in Figure 2a.

5.1.1 Várzea do Capivarita Complex paragneiss

The pelitic paragneiss (sample MN-12C) shows discontinuous banding marked by mm-thick bands and lenses of quartz + feldspar (± garnet), which alternate with cm-thick garnet-bearing, biotite-rich bands (S in Fig. 5a). A discrete, cm-spaced second foliation (C in Fig. 5a) locally drags the main banding. The second foliation is often marked by quartzo-feldspathic leucosome. The

leucosome was alternately emplaced along the two foliations, suggesting synkinematic melt mobility. The foliations are therefore interpreted to represent an S-C pair indicative of top-to-the-NW kinematics, in agreement with other kinematic indicators reported for D_1 (Martil et al., 2011, 2017; Martil, 2016).

Figure 5

At micro-scale, a sub-millimetric compositional banding is given by alternating leucosome and melanosome bands (Fig. 5b), the latter containing biotite, cordierite and garnet. Mineral chemistry is presented in Table 1.

Lepidoblastic biotite flakes are less than 250 μm in size, aligned in the main banding and defining the main folation (Fig. 6a). Round biotite crystals form inclusions in garnet and cordierite. Accessory ilmenite is found in close association with biotite. Biotite compositional parameters range from Al^T = 3.15 to 3.27 a.p.f.u. and X_{Mg} (Mg/Mg+Fe) = 0.33 – 0.37. Composition of biotite inclusions in garnet and cordierite is not different from biotite along the main fabric.

Figure 6

Garnet porphyroblasts (up to 1.5 mm in size – Fig. 6a) are widespread, and their boundaries are either irregular or straight against the melanosome matrix minerals (Fig. 6a and 6b). Some melanosome garnets show embayed contacts with cordierite (Fig. 6b). Mineral inclusions in garnet are aligned parallel with the matrix main foliation (Fig. 6a). Garnet composition (Table 1) recalculated to proportions of end-members is: almandine 0.82 – 0.84, pyrope 0.10 – 0.13, grossular 0.03, and spessartine 0.02 – 0.03, independent of crystal size or position in the sample. The analysed crystals are homogeneous.

Cordierite porphyroblasts up to 2 mm large are found in some melanosome bands either as elongate grains and aggregates (Fig. 6a to c) or as more equant grains along leucosome bands (Fig. 5b). Cordierite crystals from the leucosome are strongly pinnitized, whilst melanosome cordierite is preserved. Marginal recrystallization is locally observed. Cordierite in melanosome contains 30 – 100 μm large inclusions of green spinel (Fig. 6b and c). Spinel forms well-

aligned, elongate (Fig. 6a and b) or equant, randomly oriented crystals (Fig. 6c) interpreted as intergrowths. Cordierite also encloses aligned biotite inclusions interpreted as relics of pre-existing biotite-rich matrix (Fig. 6a and b). In the studied sample, sillimanite was only observed as relict aggregates included in cordierite (inset in Fig. 6c), whereas other metasedimentary samples from VCC have sillimanite as a main constituent (Gross. et al., 2006; Bom et al., 2014; Philipp et al., 2016; Costa et al., 2020).

Table 1

Spinel is found solely as inclusions in cordierite. This feature is common in VCC metasedimentary rocks (Gross et al., 2006; Philipp et al., 2016; Costa et al., 2020). The observed intergrowth is similar to the silica-defficient spinel-bearing ocellae described by Harris and Holland (1984), indicative of metamorphic conditions of 750 ± 50 °C and pressures up to 4.5 Kbar. Such SiO_2-subsaturated domains were considered as closed system (restricted in scale by the slow chemical diffusion of ions). The compositional domains were analysed by means of compositional mapping (similar to the approach adopted by Tajčmanová et al., 2007 and Costa et al., 2020) (Fig. 6b) in order to obtain system compositions suitable for modelling of stabilization of the cordierite + spinel assemblage. Cordierite X_{Mg} values are between 0.53 and 0.57, whereas spinel shows constant X_{Mg} of 0.12 – 0.13 (see Table 1).

5.1.2 Cerro da Árvore Complex schist

Garnet-staurolite-quartz-muscovite schist (sample MAB-52A) is a metapelitic rock from the Cerro da Árvore Complex (Fig. 7a). Muscovite-rich layers containing staurolite (up to 2 mm – Fig. 7b) and garnet (3 to 5 mm – Fig. 7c and 7d) porphyroblasts alternate with lenticular, quartz-rich layers along the main schistosity. Compositional banding is interpreted either as partially transposed, relict sedimentary layering, or pre- to synkinematic veins. Regional schistosity dips 5° to 30°, mainly to NE, and sometimes contains a slightly oblique mineral lineation marked by muscovite trails or staurolite, and more rarely quartz stretching lineation. Mineral chemistry is shown in Table 2.

Muscovite makes up to 50% of the rock volume, with 0.5 mm-long crystals sections aligned in the schistosity plane. Its silicon content is between 6.0 and 6.2 apfu.

Figure 7

Table 2

Garnet forms mostly equant, up to 5 mm-large porphyroblasts (Fig. 7c and d). The crystals commonly show sigmoidal quartz and ilmenite inclusion trails that mark the porphyroblast rotation relative to the external matrix foliation during growth (Fig. 7d). Garnet shows consistent zoning, with core composition almandine 0.73 – 0.75, spessartine 0.14 – 0.16, grossular 0.05 – 0.06, pyrope 0.06, and rim composition almandine 0.76 – 0.77, spessartine 0.11 – 0.12, grossular 0.04 – 0.05, pyrope 0.06 – 0.07.

Staurolite porphyroblasts are numerous along some foliation levels (Fig. 7b). They are strongly to completely replaced by fine-grained white mica pseudomorphs (*ca.* 2 mm), but many preserve unaltered cores (up to 1 mm), where staurolite can be recognized (Fig. 7b inset). Staurolite X_{Mg} is regularly between 0.11 and 0.13.

Quartz layers have irregular thickness and lenticular shape. Crystals are 0.05 to 0.3 mm long, many of them are equant and polygonal.

Biotite X_{Mg} is 0.38, while Al^{T} = 3.48 – 3.60 a.p.f.u. Both biotite and chlorite are late- to post-kinematic and overgrow the main schistosity. Chlorite forms radial aggregates up to 1 mm large (Fig. 7c and 7d).

Kinematic indicators observed in XZ-parallel sections include discrete shear bands (Fig. 7b), rotated garnet porphyroblasts with internal foliation (Fig. 7d) and asymmetric pressure shadows containing mainly quartz (Fig. 7c), and sheared mica aggregates. Kinematic indicators consistently show an oblique, tangential, dextral with top-to-the-SE sense of shear. On the other hand, observations from a sample collected in a neighbouring outcrop indicate opposite shear sense (towards NW).

Cerro da Árvore Complex metapelites in the studied area locally contain up to 10 cm long, post-kinematic andalusite porphyroblasts (Fig. 8a), which overgrow

the main schistosity (Lenz, 2006). Prismatic andalusite crystals are subhedral, and contain staurolite inclusions locally protected from replacement by white mica (Fig. 11b). Andalusite porphyroblasts are partly aligned N-S, subparallel to discrete, dm-spaced subvertical fractures, which are attributed to the Passo do Marinheiro Fault (see Fig. 2a).

Figure 8

5.2 Peak metamorphic conditions of the Várzea do Capivarita Complex

Calculated P-T pseudosection using the whole-rock composition of the sample MN-12C (Fig. 9) indicates that the assemblage Bt + Crd + Grt + Qtz + Kfs + Pl + melt is stable from 3.5 to 4.8 Kbar, in the temperature range of 760 – 830°C. The presence of ilmenite is predicted at slightly higher temperature or lower pressure. The appearance of spinel solely as inclusions in cordierite grains in this sample is in agreement with the absence of this mineral in the calculated pseudosection. The same is valid for sillimanite, so the resulting matrix mineral assemblage is sillimanite-free. Isopleths for garnet end-members almandine (0.76 – 0.77), pyrope (0.10 – 0.14), spessartine (0.025 – 0.03) and for X_{Mg} values of cordierite (0.52 – 0.54) and biotite (0.33 – 0.36) overlap at 790 – 820°C and 4.4 – 4.8 Kbar. The model does not predict almandine content higher than 0.77, although the range 0.82 to 0.84 was measured in the sample.

Figure 9

5.3 Várzea do Capivarita Complex exhumation conditions

The crystallization of spinel in the sample MN-12C was modelled by using an estimated bulk composition of the cordierite + spinel domain (area shown in Fig. 6b) considered as a closed system. The model (Fig.10) predicts the stabilization of spinel below *ca.* 3.7 – 6.0 kbar depending on the metamorphic temperature, in a wide PT field of the equilibrium assemblage Crd + Sp + Grt + Sil + Kfs. The isopleths for X_{Mg} of cordierite (0.56) and X_{Mg} spinel (0.13) and an additional curve corresponding to 1 vol.% of sillimanite suggest stabilization of spinel at *ca.* 660 to 680°C and 2.5 to – 3.4 kbar (Fig. 10).

The evolution of modal composition of the domain was modelled systematically with decreasing pressure and temperature. Close to the estimated whole-rock peak metamorphic conditions (800°C/4.6 Kbar – see Fig. 9), the estimated volume percentage of the minerals is $Crd_{58.34}Sp_{2.67}Grt_{20.5}Sil_{17}Kfs_{1.4}$, whereas at the estimated equilibration conditions of 680°C and 3 kbar the volume proportions change to $Crd_{88}Sp_{8.5}Grt_{1.5}Sil_{0.72}Kfs_{1.2}$. Small amounts of modelled K-feldspar are interpreted as an artefact caused by small amounts of potassium from biotite in the mapped area together with modelling under anhydrous conditions.

Figure 10

5.4 Cerro da Árvore Complex progressive metamorphic conditions

The pseudosection for the garnet-staurolite-quartz-mica schist (MAB-52A) presented in Figure 11 was calculated at H_2O-saturated conditions. The composition of garnet cores (almandine 0.73 – 0.74 and spessartine 0.14 – 0.15) points to early growth of garnet at 555 – 565°C and 5.4 – 5.7 Kbar (Fig. 10). The composition of garnet rims (almandine 0.76 – 0.77, spessartine 0.11 – 0.12 and grossular 0.04 – 0.05), staurolite (X_{Mg} = 0.11 – 0.13), muscovite (Si higher than 3.00 atoms per half-formula unit, as calculated with Perple_X), and biotite (X_{Mg} 0.37 – 0.39) constrain the metamorphic conditions of the matrix stabilization at 560 – 580°C and 5.8 – 6.3 kbar (Fig. 11). The calculated difference in PT conditions from garnet core to rim + matrix mineral assemblage is interpreted as evidence of prograde metamorphic evolution.

Figure 11

5.5 Cerro da Árvore Complex exhumation conditions

According to the pseudosection (Fig. 11), andalusite stabilized in the schist composition (MAB-52A) below 4 Kbar at *ca.* 580°C. The preserved staurolite as inclusions in andalusite (Fig. 8b) contrasts with its pervasive replacement by fine-grained white mica in the groundmass (Fig. 7b). Therefore, andalusite porphyroblasts have formed before or during retrogressive replacement of staurolite by fine-grained white mica. The occurrence of andalusite as a later

phase in these rocks points to exhumation towards low pressures (andalusite stability field).

6. Discussion

6.1 Correlation between Várzea do Capivarita and Cerro da Árvore complexes

The correlation between the Várzea do Capivarita Complex orthogneisses and the Cerro da Árvore Complex metavolcanics was first proposed by Martil et al. (2017) and Battisti et al. (2018), who compared their geochemical composition and suggested that they share similar protoliths. Both rock associations comprise medium- to high-K calc-alkaline rocks interpreted by those authors to have been formed in *ca.* 800 – 780 Ma, mature continental arc conditions (Martil et al., 2011, 2017; Battisti et al., 2018). These rocks have also been correlated with other Tonian orthogneisses exposed along the Dom Feliciano Belt hinterland (Fig. 1b), and interpreted either as the record of an arc magmatism far from the plate margin (De Toni et al., 2020a), or of a pre-collisional rift environment (Konopásek et al., 2018).

The correlation between the complexes is reinforced when provenance data by Gruber et al. (2016a, b) are considered, as they indicate maximum Tonian depositional ages for both rock units, as well as identical Mesoproterozoic and Paleoproterozoic source areas. The metamorphic ages of both units are also similar (*ca.* 660–640 Ma – Lenz, 2006; Martil, 2016; Chemale Jr. et al., 2011). The younger Várzea do Capivarita Complex ages of ca. 620 Ma (Philipp et al., 2016) and 626 - 604 Ma (Gross et al., 2006) require reinterpretation. The first one is a migmatization age, and therefore representative of the thermal relaxation period that is expected to follow the main collision (e.g. Weinberg, 2016). The second is thought to be a consequence of (i) the later closure of the garnet Sm-Nd system due to prolonged high temperature conditions related to high-T metamorphism, migmatization and recurrent magmatic activity in the area; and/or (ii) low accuracy of the two-point isochron method. Therefore, both values possibly represent younger ages than that of collisional peak metamorphism.

The structural evolution of the Cerro da Árvore Complex metavolcanic rocks near the Encruzilhada Block NW margin was compared to the Várzea do Capivarita Complex progressive deformation (Battisti et al. 2018). In summary, both complexes show an originally flat-lying metamorphic foliation (S_1) that bears highly oblique stretching lineation (L_1). Different kinematic indicators are suggestive of thrusting, and the foliation is asymmetrically folded with vergence towards the west. Along steeply-dipping short limbs a subvertical mylonitic foliation (S_2) with subhorizontal lineation (L_2) has developed as a result of strike-slip movement. Battisti et al. (2018) interpret such evolution as progressive transpressional deformation recorded in both complexes during oblique collision. The dextral character of the strike-slip movement is well documented in the Várzea do Capivarita Complex (Martil et al., 2011,2017; Martil, 2016; De Toni et al., 2016). However, Battisti et al. (2018) did not conclude about the D_2 transcurrent kinematics of Cerro da Árvore Complex metavolcanics. On the other hand, dextral shearing was reported in these rocks by Jost and Bitencourt (1980) and Jost (1981) based on the regional-scale Serra dos Pedrosas Antiform drag fold formed against the Passo do Marinheiro Fault (Fig. 2a).

A summary of the main geological features of these two units is presented in Table 3. They show that the Várzea do Capivarita and Cerro da Árvore complexes are correlative in terms of igneous activity (geochemical affinity and age), sedimentation (source areas and depositional times), deformational pattern (transpressional D_1 top-to-the-W progressively partitioned into D_2 dextral strike-slip domains) and peak metamorphic age (*ca.* 660–640 Ma). The dataset suggests that VCC and CAC protoliths were deposited in a comparable environment interpreted as a single basin or similar basins nearby, as also argued by Battisti et al. (2018). In contrast, the PT paths presented here reveal different metamorphic histories.

Table 3

6.2 Contrasting PTt paths of the Várzea do Capivarita and Cerro da Árvore complexes

A summary of new PT data integrated with published information (Fig. 12) demonstrates the contrasting, yet convergent, metamorphic PTt path of the two

studied complexes. Várzea do Capivarita Complex peak metamorphism recorded in the studied sample from the northern roof pendant is in the range of 790 – 820 °C at ca. 4.4 – 4.8 kbar (Fig. 9), which coincides with the conditions determined by Costa et al. (2020) for the southern roof pendant (location in Fig. 2a). The concordant temperature values, together with coherent structures in both roof pendants (e.g. Martil, 2016; Martil et al., 2017; Costa et al., 2020), confirms that the Encruzilhada Granite emplacement caused no significant displacement in the exposed Várzea do Capivarita crust. Temperatures may have been locally even higher due to the syntectonic emplacement of syenite magmas (De Toni et al., 2016). The timing of granulite-facies peak metamorphism in the gneisses (ca. 650 Ma according to Martil, 2016; Martil et al., 2017) and the crystallization age of the syntectonic syenite intrusions (642 ± 10 Ma; Bitencourt et al., 2016) constrain the high-T/low-P metamorphism to the 650 – 640 Ma interval.

Figure 12

Amphibolite-facies peak metamorphism was determined for the easternmost portion of Cerro da Árvore Complex. Garnet cores record an early growth at 555 – 565°C and 5.4 – 5.7 kbar, whereas rims stabilized with the matrix assemblage at 560 – 580°C and 5.8 – 6.3 kbar. This interval is in agreement with the peak metamorphic conditions estimated by Lenz (2006) for the same rocks (ca. 590°C at 5 – 6 kbar), and in closer detail reveals a burial path. Despite the high uncertainty of the metamorphic Rb-Sr age reported by Lenz (2006) (658 ± 26 Ma), synchronous metamorphism of the Cerro da Árvore and Várzea do Capivarita complexes at contrasting conditions is implied.

Exhumation conditions for the granulitic metapelite were determined from the SiO_2-subsaturated association of cordierite + spinel ± sillimanite at 660 – 720°C and 2.5 – 3.4 kbar (Fig. 10), in agreement with data from the southern roof pendant (Costa et al., 2020). The observed intergrowth is a recognized feature of rapid decompression in high-grade metasediments (e.g. Harris and Holland, 1984; Bindu, 1997; Johnson et al., 2004). Decrease in volume of garnet and sillimanite, and increase in volume of cordierite and spinel from metamorphic peak to re-equilibration conditions are in agreement with the reaction proposed

by Mezger et al. (2008) (1). Additionally, the embayed contact with garnet (Fig. 6b) and rare sillimanite aggregates included in corderite (Fig. 6c) point to these minerals as reactants for the spinel-forming reaction:

Sil + Grt = Crd + Sp (1)

The results point to a very hot crust exhumed to shallow levels, with consequently high apparent geothermal gradient preserved during decompression. The emplacement conditions of 700 – 750 °C and 3 – 4.2 kbar determined for the associated sillimanite-bearing Butiá Granite (Niessing, 2008), plotted in Figure 12, are in agreement with the exhumation path of the complex. Considering (i) the genetic link between this granite and the Várzea do Capivarita Complex partial melting as argued by Bom et al. (2014), Philipp et al. (2016); and Costa et al. (2020), (ii) the granite age (629.8 ± 6.8 Ma) and (iii) its emplacement conditions with intermediate values between those of VCC peak metamorphism and exhumation (this work and Costa et al., 2020), we can conclude that its syntectonic emplacement took place during the Várzea do Capivarita Complex exhumation. This is in agreement with the hypothesis of melt-assisted exhumation of Costa et al. (2020).

If both studied complexes originated in the same basin, which would be tectonically inverted, it is likely that during thrusting of the VCC thickened crust towards the west its overweight affected the underthrusted Cerro da Árvore Complex rocks. This caused progressively higher pressures recorded by the underthrusted CAC peak metamorphic assemblage. This thickened rock pile is the source of the very low aeromagnetic anommaly observed in the Encruzilhada Block (Fig. 4a).

Considering the small difference in estimated peak pressure of the complexes (between 1 and 1.5 kbar), it is possible that both were juxtaposed at the pressure recorded by CAC (ca. 6 kbar). In this hypothesis, both complexes may have been exhumed together, and VCC minerals reequilibrated their composition during exhumation, due to the high temperatures, while CAC peak pressure assemblages were preserved due to lower temperatures. Actually, VCC PT-path is very similar to the one for the Cerro Olivo Complex

paragneisses from Punta del Este Terrane (Uruguay), which record higher pressure peak metamorphism at 830 – 950 °C and 7 – 10 kbar, followed by near-isothermal decompression to 788 – 830 °C and 4.8 – 5.5 kbar, and retrograde conditions of 600 – 750°C and 3 – 6 kbar (Gross et al., 2009).

Várzea do Capivarita Complex metapelitic hornfelses with small andalusite crystals are found in roof pendants at the northern margin of the Piquiri Syenite Massif (Martil, 2007), and radial sillimanite is described in xenoliths found in the Arroio do Silva Pluton (Padilha et al., 2019). These are additional evidences for shallow-level and low-strain conditions in the Encruzilhada Block at this time (609 – 578 Ma). The Piquiri Syenite Massif is also responsible for thermal effects over the Cerro da Árvore Complex metavolcanics in its southwest roof pendant (Battisti et al., 2018). The large and partly aligned andalusite crystals overgrowing the Cerro da Árvore Complex metapelites (Fig. 8) are interpreted to result from the Piquiri Syenite Massif (609 – 584 Ma) or Encruzilhada Granite emplacement (≤ 578 Ma). From the abovementioned evidences it is concluded that at the time of intrusion of these granitoids, the studied complexes were already juxtaposed along the Passo do Marinheiro Fault at relatively low depth corresponding to 2.5 – 4 kbar.

6.3 Possible origins of the Várzea do Capivarita Complex anomalous geothermal gradient

Geothermal gradient as high as 50 to 60 °C/km registered in the VCC rocks (this work and Costal et al., 2020) points to a very hot collisional environment in contrast with geothermal gradients of *ca.* 30 °C/km recorded by CAC metapelites. The question is what kind of environment could explain the anomalous conditions implied by high-T/low-P metamorphism. Among the factors that may contribute to generate such extreme conditions, the correlation with large volumes of magma and concentration of heat-producing elements are considered as the key points (e.g. Clark et al., 2011; Gorczyk and Vogt, 2015). Many authors consider such conditions suggestive of an attenuated pre-collisional lithosphere with high sub-lithospheric mantle heat influx (Harris and Holland, 1984; Thompson et al., 2001; Clark et al., 2011; Fowler et al., 2015; Hyndman et al., 2015).

According to the numerical modelling of Gorczyk and Vogt (2015) based on the data from the Musgrave Intracontinental Orogeny of Central Australia, lithospheric delamination of a previously weakened back-arc region located between stronger cratonic blocks may occur during contractional deformation driven by far-field plate boundary processes. According to the authors, this may result in an extended period, up to 100 Ma, of UHT and high-T/low-P metamorphism, and abundant episodic A-type magmatism in 10 to 20 m.y. cycles.

Despite size/proportion differences, these characteristics are in good agreement with the observations and interpretations for the Encruzilhada Block, which was likely affected by pre-collisional extension in Tonian times (e.g. Konopásek et al., 2018; De Toni et al., 2020a). The block features high-T/low-P roof pendants intruded by alkaline rocks. Such rocks include syntectonic (ca. 640 Ma) and late-tectonic syenites (609 to 578 Ma), and the A-type Encruzilhada Granite, which is also considered as a record of post-collisional magmatism (*sensu* Liégeois, 1998). Evidence indicates that the mantle was possibly a shallow source for both the alkaline magmatism and the heat responsible for anomalous high geothermal gradient, possibly assisted by delamination of the lithosphere. Additionally, the Encruzilhada Block basement is Mesoproterozoic, while it is located between domains with Paleoproterozoic basement inliers (Fig. 2a). This suggests that a discontinuity in the pre-collisional lithosphere may have exerted control on the block position, which may reflect a structural heritage.

6.4 *Encruzilhada Block autochtonous origin – past and present boundaries*

Considering the previously discussed similarities (Table 3) and following previous interpretations (Battisti et al., 2018; De Toni et al., 2020a), we propose that the protoliths of the Várzea do Capivarita and Cerro da Árvore complexes represent coeval and spatially close basins, if not a single one. This basin registered igneous activity at ca. 800 – 780 Ma and sedimentation until at least ca. 730 Ma. Tonian orthogneisses along the entire Dom Feliciano Belt hinterland (Fig. 1b) represented the deeper part of this volcano-sedimentary basin, possibly formed on a highly stretched continental crust, under a high

geothermal gradient (Fig. 13a). On the other hand, the Cerro da Árvore Complex probably represented the shoulder of this basin.

Figure 13

At 660 – 640 Ma, the basin was inverted and its basement and deepest strata were tectonically juxtaposed over its shallower and colder margin (Cerro da Árvore Complex rocks) by west-verging transpression (Fig. 13b). One possible consequence of this deformation are the opposite PT-paths of the complexes, with exhumation of Várzea do Capivarita Complex rocks during thrusting, and tectonic burial of underthrust Cerro da Árvore Complex (Fig. 12).

Slow cooling and decompression progressively followed peak metamorphism of the Várzea do Capivarita Complex during exhumation and thermal relaxation, with migmatization and the origin of peraluminous granites at 630 – 620 Ma (Fig. 13c). At this time, the progressive deformation and strain partitioning activated strike-slip shear zones, which focused this magmatism along major structures of the Southern Brazilian Shear Belt. The opposite shear sense along NNW- and NE-striking shear zones, recorded by synchronous and genetically related magmatic rocks, points to the need to fit both structures in a coherent array, as discussed by Lyra et al. (2018).

Dextral shearing at *ca.* 630 Ma developed in the Butiá Granite and the Várzea do Capivarita Complex rocks focused along the Passo das Canas Shear Zone (Fig. 2a). Clockwise movement along pervasive, steeply-dipping, NNW-striking S_2 foliation, bearing sub-horizontal to NNW-plunging L_2 (Fig. 2c) has possibly helped Várzea do Capivarita Complex exhumation. Such kinematics is also coherent with the one observed at the western boundary of the Encruzilhada Block, affecting the Cerro da Árvore Complex rocks (Fig. 13d), as the dextral drag fold against Passo do Marinheiro Fault (Fig. 2a). The Dorsal de Canguçu Shear Zone has focused the sinistral shear southeast of the Encruzilhada Block, recorded by syntectonic granites crystallized at 635 – 605 Ma. Movement of the Encruzilhada Block to the south at 630 – 610 Ma is apparently necessary in order to keep strain compatibility (Jost, 1981; Lyra et al., 2018) and may be interpreted as the extrusion component of overall oblique transpression.

The contact between the studied complexes is not exposed. The modern expression of this contact is the Passo do Marinheiro Fault, which is considered to represent the reactivation of a former ductile dextral shear zone (Jost and Bitencourt, 1980; Jost, 1981). Since both complexes have originally subhorizontal, NNW-striking foliations (S_1) with highly oblique lineations related to thrusting (Fig. 2b, c and d), the original contact may have been subhorizontal, further transposed by subvertical structures of the same strike (S_2). It is also possible that the original contact was subvertical, since S_2 was active during emplacement of the Butiá Granite and exhumation of the VCC along the Passo das Canas Shear Zone. An additional argument comes from the aeromagnetometric image (Fig. 4a), where a very low signal in the area of the Encruzilhada Block suggests a thick sedimentary pile below surface, favouring the hypothesis of an originally subhorizontal contact surface between the complexes, which may be preserved in depth (Fig. 13).

It is noteworthy that the southeastern boundary of the Encruzilhada Block is the Dorsal de Canguçu Shear Zone (Fig. 2a). On the other hand, the Porto Alegre Lineament represents the boundary between the lowermost magnetic domain and the eastern medium- to high-signal domains Md2a, Md3a and Md3b, respectively (Fig. 4d). The low magnetic area is mostly interpreted to represent a thick supracrustal rock pile, possibly tectonically thickened due to thrusting of the Várzea do Capivarita Complex over the Cerro da Árvore Complex rocks. Furthermore, the syntectonic granites along the major NE-striking shear zones are part of the same magnetic domain as the Encruzilhada Block (Gd3 is inside Md2a in Fig. 4d). This is possibly due the crustal origin of these granites as reworked metasedimentary sources (Bom et al., 2014; Philipp et al., 2016; Costa et al., 2020), and to their low magnetic mineral contents (e.g. Lyra et al., 2018).

Late-tectonic intrusions along the western Encruzilhada Block boundary have obliterated the original contact between the studied complexes after *ca.* 610 Ma, as well as the original boundary of the block itself. The Piquiri Syenite Massif, with its metavolcanic roof pendant studied by Battisti et al. (2018), is also intrusive in the Várzea do Capivarita Complex (Stabel et al., 2001; Martil, 2007; Rivera, 2019) and crosscuts the Passo do Marinheiro Fault (Fig. 2a and 13e), being not significantly affected by faulting. This evidence suggests that there

has been no significant activity along the fault after emplacement of the massif. Sbaraini et al. (2020) suggested that the syenite massif was emplaced under extension, while for Rivera (2019) the emplacement was controlled by dextral trantension along the Passo das Canas Shear Zone. Both alternatives would explain its structural control and absence of solid-state deformation imprint.

The presence of late-Ediacaran fault-bounded basins in the Tijucas Fold Belt is an additional argument in favour of extensional tectonics west of the Encruzilhada Block at this time (Fig. 2a and 13f). Recent work by Fambrini et al. (2018) about Ediacaran sedimentary basins west of the Encruzilhada Block points out that the Piquiri Syenite Massif must have been exposed to subaerial erosion at the time of basin deposition, which is indicated by many clasts of its rock types found in the conglomerates. This also points to the fact that erosion has played an important role in the Encruzilhada Block exhumation, and that no significant horizontal displacement has occurred along the main faults after sedimentation, since the local sedimentary source is found very close to the basin. The same authors also recognized that from bottom to top, provenance data indicate progressive denudation of deeper units (metavolcanosedimentary, plutonic), which suggests rapid relative uplift of the source area.

The emplacement of the Encruzilhada Granite (≤ 578 Ma, Padilha et al., 2019) is interpreted by Jacobs et al. (2018) to have been controlled by previous discontinuities as the Dorsal de Canguçu Shear Zone and the Passo do Marinheiro Fault (Fig. 2 and 13f). At this time, both studied complexes are thought to have been side-by-side at shallow crustal levels (less than 3.5 kbar or 13 km), as shown by metamorphic assemblages and its convergent PT-paths (Fig. 12).

Observations recently made by the authors on the Encruzilhada Granite near the western margin of the Encruzilhada Block, north of Cerro da Árvore Fault (Fig. 2a), have not shown any deformational feature in the granite. What is rather seen is the apparent structural control of the intrusion by a pre-existing NS-striking subvertical structure that conditions emplacement of aplitic and pegmatitic veins and quartz venules.

Taken together, the evidence suggests that neither the Piquiri Syenite Massif nor the Encruzilhada Granite intrusion were accompanied or followed by significant displacement along the Passo do Marinheiro Fault, but were rather

conditioned by this structure. The large, partly NS-aligned andalusite crystals grown over the schists near the Passo do Marinheiro Fault (Fig. 2a) are interpreted to result from fluids related to one of these intrusions.

6.5 *Transpressive intracontinental shear zones within the Dom Feliciano Belt orogenic evolution*

Recent works correlated the hinterland and foreland of Dom Feliciano Belt in Uruguay (Oriolo et al., 2016a), Rio Grande do Sul (Battisti et al., 2018) and Santa Catarina (Florisbal et al., 2012; Bruno et al., 2018; De Toni et al., 2020b) sectors (Fig. 1b), and proposed a common tectonic history for these domains at least since 650 - 630 Ma. In the three sectors, both domains exhibit a coherent transpressional progressive deformation of top-to-the-W/NW oblique thrust, responsible for the juxtaposition of high-grade hinterland and medium- to low-grade foreland, as exemplified in this study. During progressive deformation, strain partitioning led to strike-slip movement along shear zones that controlled the post-collisional magmatism in the hinterland batholiths, modifying its original boundaries with the foreland Tijucas Fold Belt (e.g. Fernandes and Koester, 1999; Bitencourt and Nardi, 2000; Florisbal et al., 2012; De Toni et al., 2020b; Vieira et al., 2020).

The intracontinental character of the Major Gercino Shear Zone in Santa Catarina (Fig. 1b) was suggested by Florisbal et al. (2012), who correlated post-collisional granites emplaced within that zone with those crosscutting the foreland. Investigation of basement rocks from hinterland and foreland infrastructure revealed that similar metamorphic conditions and partial melting affected both domains at ca. 650 – 635 Ma (De Toni et al., 2020b). Moreover, the structural evolution of both domains is conceived in a model of overall oblique transpression progressively partitioned into dextral strike-slip along the Major Gercino Shear Zone, whilst contractional and dip-slip deformation were partitioned respectively into the foreland infra- and suprastructure. Additionally, geophysical potential data presented by Bruno et al. (2018) suggests an alternative location of the suture farther north.

In Uruguay, the intracontinental character of the Sierra Ballena Shear Zone, at the boundary of hinterland and foreland, was pointed out by Oriolo et al. (2016a, 2016b, 2017), and a coherent transpressive deformation pattern is presented

for both domains (630 – 595 Ma). The suture in this sector is considered to be located farther west, between the Rio de la Plata Craton and Nico Perez Terrane (Fig. 1b).

The same correlation criteria is valid in the Rio Grande do Sul sector of Dom Feliciano Belt, where the Dorsal de Canguçu Shear Zone is conceived as an intracontinental structure (Fernandes et al., 1995a,b; Fernandes and Koester, 1999). The intracontinental character of major shear zones of the Southern Brazilian Shear Belt (Bitencourt and Nardi, 2000) requires a review of the existing evolutionary models for the Dom Feliciano Belt in the context of Western Gondwana amalgamation, including its compatibility with plate margin geodynamics.

7. Conclusions

The Encruzilhada Block is an autochtonous tectonic entity of mixed characteristics and units correlated to both the foreland (Tijucas Fold Belt) and the hinterland (Pelotas Batolith) of Dom Feliciano orogen. Tectonic analysis of lineaments confirms the structural similarity of the Encruzilhada Block with the foreland, with predominantly NNW- to NNE-trending lineaments that are in sharp contrast with the NE-striking ones in the hinterland. From a geophysical perspective, the block has similar characteristics to both the foreland, in terms of low to medium aeromagnetometric signal due to correlated thick metamorphosed supracrustal sequences, and to the hinterland, in terms of high aerogammaspectrometric signal due to correlated abundant post-collisional magmatism (Fig. 2a and 4).

Cerro da Árvore and Várzea do Capivarita complexes are correlated by multiple criteria, as precursor basins and protoliths of Tonian age, as well as coherent transpressional deformation at late Cryogenian times (Table 3). Their PT paths are contrasting, yet convergent (Fig. 12). Várzea do Capivarita Complex was subject to high-T/low-P granulite-facies metamorphism and partial melting at 790 – 820 °C / 4.4 – 4.8 kbar at 650 – 640 Ma, which confirms and refines previous estimates. On the other hand, Cerro da Árvore Complex was subject to amphibolite facies prograde metamorphism, with early growth of garnet cores at 555 – 565°C / 5.4 – 5.7 kbar, and peak metamorphism at 560 – 580°C / 5.8 – 6.3 kbar at *ca.* 660 Ma. The data are summarized in a model, in which both

complexes represent originally different depths of a correlated, if not the same, volcano-sedimentary basin inverted during oblique collision at ca. 650 Ma. At this time, Cerro da Árvore Complex records underthrusting and tectonic burial under the middle–lower continental crust represented by the Várzea do Capivarita Complex.

Várzea do Capivarita Complex exhumation is registered in SiO_2-subsaturated domains with cordierite + spinel ± sillimanite intergrowths that record metamorphic conditions of 660 – 720°C / 2.5 – 3.4 kbar at *ca.* 630 Ma. The high geothermal gradient (50 – 60°C/km) recorded during the exhumation process is attributed to a pre-collisional phase of ductile thinning of the lithosphere followed by basin tectonic inversion, and/or to syncollisional lithosphere delamination.

Late-tectonic intrusions are responsible for obliterating the original contact between the two complexes and the western boundary of the Encruzilhada Block. Contact metamorphism features point out the fact that both Várzea do Capivarita and Cerro da Árvore complexes were side-by-side at the time of the late-tectonic intrusions. Intrusive contact relationships of the Piquiri Syenite Massif and its position relative to the Passo do Marinheiro Fault suggest that juxtaposition of the complexes occurred during or before syenite emplacement.

The autochtonous character of the Encruzilhada Block discourages the use of the term terrane to refer to it, since the neigbouring blocks share many characteristics, and therefore cannot be classified as exotic. The results also discourage interpretation of the Dorsal de Canguçu Shear Zone as a suture. The same holds for any of the other regional structures of the Southern Brazilian Shear Belt separating hinterland and foreland of Dom Feliciano Belt. The presented data validate the correlation of ca. 800 – 780 Ma metavolcanic rocks (foreland) and orthogneisses (block and hinterland) from the three domains, and point towards a common pre-collisional history, which should be considered independent of what tectonic model is adopted. The unraveled autochtonous origin of the Encruzilhada Block is viewed as a key-piece towards understanding of the Dom Feliciano-Kaoko-Gariep orogenic system evolution, as well as the importance of intracontinental shear zones and orogenic processes linked to plate margin geodynamics during Western Gondwana assembly.

CRediT author statement

Giuseppe Betino De Toni: Conceptualization; Methodology; Formal analysis; Investigation; Writing - Original Draft; **Maria de Fátima Bitencourt**: Supervision; Writing - Review & Editing; Project administration; Funding acquisition; **Jiří Konopásek**: Supervision; Validation; Writing - Review & Editing; Project administration; Funding acquisition; **Matheus Ariel Battisti**: Investigation; **Elisa Oliveira da Costa**: Validation; **Jairo Francisco Savian:** Data Curation; Validation; Resources.

Declaration of interests

The authors declare that they have no known competing financial interests or personal relationships that could have appeared to influence the work reported in this paper.

Acknowledgements

The authors acknowledge financial support of the Brazilian National Research Council (CNPq) through productivity grant to MF Bitencourt (311486/2015-0) and PhD scholarship (141011/2015-7) to GB De Toni, as well as financial support organized within the framework of CAPES (Brazil) – SIU (Norway) cooperation program (CAPES - 88881.117872/2016-01 and 88887.141226/2017-00, SIU – TF-2016-CAPES-SIU/10024). J Konopásek appreciates financial support of the Czech Science Foundation (grant no. 18-24281S). Diego Lyra is acknowledged for help with Geosoft. João VT Mello and Rafael P Ribeiro are acknowledged for help with ASTER image processing. Kai Neufeld is acknowledged for help with SEM compositional mapping at UiT. We are also grateful to Susan Drago for her kind help during microprobe analysis at UFRGS. To all participants of UFRGS mapping courses (2006 – 2011): thank you!

References

Almeida, F.F.M., de Brito Neves, B.B., Carneiro, C.D.R., 2000. The origin and evolution of south american platform. Earth-Science Reviews, 50, 77-111.

Arena, K.R., Hartmann, L.A., Lana, C., 2016. Evolution of Neoproterozoic ophiolites from the southern Brasiliano Orogen revealed by zircon U–Pb–Hf isotopes and geochemistry. Precambrian Research 285, 299–314

Babinski, M., Chemale Jr., F., Van Schmus, W.R., Hartmann, L.A.., and Silva, L.C. da, 1996. U-Pb and Sm-Nd geochronology of the Neoproterozoic granitic-gneissic Dom Feliciano Belt, southern Brazil. Journal of South American Earth Sciences, 10(3-4), 263–274.

Basei, M.A.S., Frimmel, H.E., Nutman, A.P., Preciozzi, F., Jacob, J. 2005. The connection between the Neoproterozoic Dom Feliciano (Brazil/Uruguay) and Gariep (Namibia/South Africa) orogenic belts. Precambrian Research, 139, 139–221.

Basei, M.A.S., Frimmel, H.E., Nutman, A.P., Preciozzi, F., 2008. West Gondwana amalgamation based on detrital zircon ages from Neoproterozoic Ribeira and Dom Feliciano belts of South America and comparison with coeval sequences from SW Africa. *in*: Pankhurst, R.J., Trouw, R.A.J., Brito Neves, B.B., De Wit, M.J. (eds) West Gondwana: Pre-Cenozoic Correlations Across the South Atlantic Region. Geological Society, London, Special Publications, 294, 239–256.

Battisti, M.A.B., Bitencourt, M.F., De Toni, G.B., Nardi, L.V.S., Konopásek, J., 2018. Metavolcanic rocks and orthogneisses from Porongos and Várzea do Capivarita complexes: A case for identification of tectonic interleaving at different crustal levels from structural and geochemical data in southernmost Brazil. Journal of South American Earth Sciences, 88, 253-274.

Bindu, R.S., 1997. Granulite Facies Spinel-Cordierite Assemblages from the Kerala Khondalite Belt, Southern India. Gondwana Research, 1(1), 121-128.

Bitencourt, M.F., Nardi, L.V.S., 2000. Tectonic setting and sources of magmatism related to the Southern Brazilian Shear Belt. Revista Brasileira de Geociências 30, 186–189.

Bitencourt M.F., Nardi L.V.S., Florisbal L.M., Heaman L.M., 2015. Geology, geochronology and petrogenesis of a Neoproterozoic, syntectonic sillimanite-muscovite-biotite granite from southernmost Brazil. In: 8th Hutton Symposium on Granites and Related Rocks, Book of Abstracts.

Bitencourt, M.F., De Toni, G.B., Florisbal, L.M., Nardi, L.V.S., Martil, M.M.D., Heaman, L., DuFrane, A., Chemale Jr., F., 2016. Timing of syenitic syntectonic

magmatism as a record of strain partitioning during Cryogenian collisional transpressive regime in southernmost Brazil. *in:* Primer Simposio de Tectonica Sudamericana – Acta. Santiago, Chile. 206 p.

Bom, F.M., Philipp, R.P., Zvirtes, G. 2014. Origem e evolução do Complexo Várzea do Capivarita, Encruzilhada do Sul, RS. Pesquisas em Geociências, 41(2), 131-153.

Borba, A.W., Maraschin, A.J., Noronha, F.L., Casagrande, J., Mizusaki, A.M.P., 2007. Provenance of the sedimentary rocks of the Bom Jardim Group (Neoproterozoic, Southern Brazil): evidence from petrography, geochemistry and neodymium isotopes. Latin American Journal of Sedimentology and Basin Analysis. 14(1), 25-42.

Brown, G.C., Hughes, D.J., Esson, J. 1973. New RFX data retrieval techniques and their application to U.S.G.S. standard rocks. Chemical Geology 11, 223-229.

Bruno, H., Almeida, J., Heilbron, M., Salomão, M., Cury, L., 2018. Architecture of major precambrian tectonic boundaries in the northern part of the Dom Feliciano Orogen, southern Brazil: Implications for the West Gondwana amalgamation. Journal of South American Earth Sciences, 86, 301-317.

Burton-Johnson, A., Riley, T.R., 2015. Autochthonous v. accreted terrane development of continental margins: a revised in situ tectonic history of the Antarctic Peninsula. Journal of the Geological Society, 172, 822-835.

Chemale Jr., F., 2000. Evolução Geológica do Escudo Sul-rio-grandense. In: Geologia do Rio Grande do Sul. CIGO/UFRGS, Porto Alegre, 2002. 444 p.

Chemale Jr. F. Philipp R.P., Dussin I., Formoso M.L.L., Kawashita K., Berttotti A.L. 2011. Lu-Hf and U-Pb age determination of the Capivarita Anorthosite, Dom Feliciano Belt, Brazil, Precambriam Research, 186, 117-126.

Clark, C., Fitzsimons, I.C., Healy, D. and Harley, S.L., 2011. How does the continental crust get really hot? Elements, v. 7(4), 235-240.

Costa, E.O, Gomes, E.M., Bitencourt, M.F., De Toni, G.B., Nardi, L.V.S., 2020. Reassessing the PT conditions of Neoproterozoic collisional metamorphism and partial melting in southernmost Brazil. Journal of South American Earth Sciences, 100, 102584.

CPRM. 2010. Projeto Aerogeofísico Escudo do Rio Grande do Sul. LASA PROSPECÇÕES S.A., Relatório Técnico, 260 pp.

Coggon, R., Holland, T.J.B. ,2002. Mixing properties of phengitic micas and revised garnet-phengite thermobarometers. Journal of Metamorphic Geology, 20, 683-696.

Connolly, J.,A.,D., 2005. Computation of phase equilibria by linear programming: a tool for geodynamic modeling and its application to subduction zone decarbonation. Earth and Planetary Science Letters, 236(1–2), 524–541.

De Toni, G.B., Bitencourt, M.F., Nardi, L.V.S., 2016. Strain partitioning into dry and wet zones and the formation of Ca-rich myrmekite in syntectonic syenites: a case for melt-assisted dissolution replacement creep under granulite facies conditions. Journal of Structural Geology, 91:88-101.

De Toni, G.B., Bitencourt, M.F., Nardi, L.V.S, Florisbal, L.M., Almeida, B.S., Geraldes, M., 2020a. Dom Feliciano Belt orogenic cycle tracked by its pre-collisional magmatism: the Tonian (ca. 800 Ma) Porto Belo Complex and its correlations in southern Brazil and Uruguay. Precambrian Research, 342, 105702.

De Toni, G.B., Bitencourt, M.F., Konopásek, J., Martini, A., Andrade, P.H.S., Florisbal, L.M., de Campos, R.S., 2020b. Transpressive strain partitioning between the Major Gercino Shear Zone and the Tijucas Fold Belt, Dom Feliciano Belt, Santa Catarina, southern Brazil. Journal of Structural Geology, 136, 104058.

Dragone, G N, Ussami, N, Gimenez, M E, Klinger, F G L, Chaves, C A M, 2017. Western Parana suture/shear zone and the limits of Rio Apa, Rio Tebicuary and Rio de la Plata cratons from gravity data. Precambrian Research, 291, 162-177.

ERDAS Imagine, 2014. https://www.hexagongeospatial.com/products/power-portfolio/erdas-imagine

Fambrini, G.L., Almeida, R.P., Janikian, L., Riccomini, C., Proveniência e paleocorrentes de conglomerados e arenitos do Grupo Santa Bárbara (Ediacarano) no Vale do Piquiri, Sub-bacia Camaquã Oriental, RS: implicações tectônicas. Geologia USP Série Científica, 18(1), 149-183.

Fernandes, L.A.D., Koester, E., 1999. The Neoproterozoic Dorsal de Canguçu strike-slip shear zone: its nature and role in the tectonic evolution of southern Brazil. Journal of African Earth Sciences, 29, 3–24.

Fernandes, L.A.D., Menegat, R., Costa, A.F.U., Koester, E., Kramer, G., Tommasi, A., Porcher, C.C., Ramgrab, G.E., Camozzato, E., 1995a. Evolução

tectônica do Cinturão Dom Feliciano no Escudo Sul-rio-grandense: Parte I – uma contribuição a partir do registro geológico. Revista Brasileira Geociências 25, 351-374.

Fernandes, L.A.D., Menegat, R., Costa, A.F.U., Koester, E., Kramer, G., Tommasi, A., Porcher, C.C., Ramgrab, G.E., Camozzato, E., 1995b. Evolução tectônica do Cinturão Dom Feliciano no Escudo Sul-rio-grandense: Parte II – uma contribuição a partir das assinaturas geofísicas. Revista Brasileira Geociências 25, 375-384.

Florisbal, L.M., Janasi, V.A., Bitencourt, M.F., Heaman, L.M., 2012. Space–time relation of post-collisional granitic magmatism in Santa Catarina, southern Brazil: U–Pb LA-MC-ICP-MS zircon geochronology of coeval mafic-felsic magmatism related to the Major Gercino Shear Zone. Precambrian Research, 216, 132–151.

Fossen, H., Cavalcante, C., Konopásek, J., Meira, V.T., Almeida, R.P., Hollanda, M.H.B.M., Trompette, R., 2020. A critical discussion of the subduction-collision model for the Neoproterozoic Araçuaí-West Congo orogeny. Precambrian Research, 343, 105715.

Fowler, A., Hassen, I., Hassan, M., 2015. Tectonic evolution and setting of the Sa'al Complex, southern Sinai, Egypt: A Proterozoic continental back-arc rift model. Journal of African Earth Sciences, 104, 103-131.

Fuhrman, M.L.,Lindsley, D.H., 1988. Ternary-Feldspar Modeling and Thermometry. American Mineralogist 73, 201-15.

GEOSOFT. 2005. Sharpening using interactive reweighting inversion, Oasis Montaj best practice guide. http://www.geosoft.com

Gorczyk, W., Vogt, K., 2015. Tectonics and melting in intra-continental settings. Gondwana Research, 27, 196-208.

Gregory, T.R., Bitencourt, M.F., Nardi, L.V.S, Florisbal, L.M., 2017. Petrogenesis of metamorphosed Paleoproterozoic, arc-related tonalites, granodiorites and coeval basic to intermediate rocks from southernmost Brazil, based on elemental and isotope geochemistry. Lithos, 277, 72-91.

Gregory, T.R.; Bitencourt, M.F.; Nardi, L.V.S.; Florisbal, L.M., Chemale Jr. 2015. Geochronological data from TTG-type rock associations of the Arroio dos Ratos Complex and implications for crustal evolution of southernmost Brazil in Paleoproterozoic times. Journal of South American Earth Sciences, 57:49-60.

Gross, A.O.M.S., Droop, G.T.R., Porcher, C.C., Fernandes, L.A.D., 2009. Petrology and thermobarometry of mafic granulites and migmatites from the Chafalote Metamorphic Suite: New insights into the Neoproterozoic P–T evolution of the Uruguayan—Sul-Rio-Grandense shield. Precambrian Research, 170, 157-174.

Gross, A.O.M.S., Porcher, C.C., Fernandes, L.A.D., Koester, E., 2006. Neoproterozoic lowpressure/high-temperature collisional metamorphic evolution in the Varzea do Capivarita metamorphic suite, SE Brazil: thermobarometric and Sm/Nd evidence. Precambrian Research 147, 41–64.

Gruber, L., Porcher, C.C., Geller, H., Fernandes, L.A.D, Koester, E., 2016b. Geochronology (U-Pb) and isotope geochemistry (Sr/Sr and Pb/Pb) applied to the Várzea do Capivarita Metamorphic Suite, Dom Feliciano Belt, Southern Brazil: Insights and paleogeographical implications to West Gondwana evolution. Geochimica Brasiliensis 30(1): 55 – 71.

Gruber, L., Porcher, C.C., Koester, E., Bertotti, A.L., Lenz, C.,Fernandes, L.A.D, Remus, M.V.D, 2016a. Isotope Geochemistry and Geochronology of Syn-Depositional Volcanism in Porongos Metamorphic Complex, Santana Da Boa Vista Antiform, Dom Feliciano Belt, Brazil: Onset of an 800 Ma Continental Arc. Journal of Sedimentary Environments, 1(2):202-221.

Harris, N.B.W., Holland, T.J.B., 1984. The significance of cordierite-hypersthene assemblages from the Beitbridge region of the Central Limpopo Belt: evidence for rapid decompression in the Archaen? American Mineralogist, 69:1037-1049.

Hartmann, L.A., Lopes, W.R., Savian, J.,F., 2016. Integrated evaluation of the geology, aerogammaspectrometry and aeromagnetometry of the Sul-Riograndense Shield, southernmost Brazil. Anais da Academia Brasileira de Ciências, 188(1), 75-92.

Hartmann, L. A., Santos, J. O. S., Mcnaughton, N. J., Vasconcellos, M.A.Z., Silva, L.C. 2000. Ion microprobe (SHRIMP) dates complex granulite from Santa Catarina, southern Brazil. Anais da Academia Brasileira de Ciências, Rio de Janeiro, 72, 560-572.

Hasui, Y., Carneiro, C.D.R. And Coimbra, A.W., 1975. The Ribeira folded belt. Brazilian Journal of Geology, 5, 257-266.

Heilbron, M., Valeriano, C.M., Peixoto, C., Tupinambá, M., Neubauer, F., Dussin, I., Corrales, F., Bruno, H., Lobato, M., Almeida, J.C.H., Silva, L.G.E.,

2020. Neoproterozoic magmatic arc systems of the central Ribeira belt, SE-Brazil, in the context of the West-Gondwana pre-collisional history: A review. Journal of South American Earth Sciences, 103, 102710.

Höfig, D.F., Marques, J.C., Basei, M.A.S., Giusti, R.O., Kohlrausch, C., Frantz, J.C., 2017. Detrital zircon geochronology (U-Pb LA-ICP-MS) of syn-orogenic basins in SW Gondwana: new insights into the cryogenian-ediacaran of Porongos complex, Dom Feliciano belt, southern Brazil. Precambrian Research, 306, 189-208.

Holland T., Baker J.,Powell R., 1998. Mixing properties and activity-composition relationships of chlorites in the system MgO-FeO-Al2O3-SiO2-H2O. European Journal of Mineralogy 10, 395-406.

Holland T.,Powell R. ,1996. Thermodynamics of order-disorder in minerals. 2. Symmetric formalism applied to solid solutions. American Mineralogist, 81, 1425-37.

Holland T.J.B., Powell R., 1998. An internally consistent thermodynamic data set for phases of petrological interest. Journal of Metamorphic Geology, 16, 309–343.

Holland T.,Powell R., 2001. Calculation of phase relations involving haplogranitic melts using an internally consistent thermodynamic dataset. Journal of Petrology, 42, 673-83.

Hyndman, R.D., Currie, C.A., Mazzotti, S.P., 2005. Subduction zone backarcs, mobile belts and orogenic heat. GSA Today, 15.

Jacobs, M. G., Philipp, R.P., Koester, E., Nardi, L.V.S., 2018. Magmatismo máfico associado ao Granito Encruzilhada do Sul, RS: implicações para a geração do magmatismo granítico pós-colisional do Cinturão Dom Feliciano. Pesquisas em Geociências, 46, e0669. DOI: https://doi.org/10.22456/1807-9806.88648

Johnson, T., Brown, M., Gibson, R., Wing, B., 2004. Spinel–cordierite symplectites replacing andalusite: evidence for melt-assisted diapirism in the Bushveld Complex, South Africa. Journal of Metamorphic Geology, 22:529–545.

Jost, H., Bitencourt, M.F., 1980. Estratigrafia e tectônica de uma fração da Faixa de Dobramentos Tijucas no Rio Grande do Sul. Acta Geológica Leopoldensia, 4(7), 27-60. São Leopoldo, RS, Brazil.

Jost, H., 1981. Geology and Metallogeny of the Santana da Boa Vista Region, Southern Brazil. Unpublished PhD thesis. University of Georgia, USA. 220 p.

Jost, H., Hartmann, L.A., 1984. Província Mantiqueira – Setor Meridional. *in:* Pré-Cambriano do Brasil. Coord.: Almeida, F.F.M., Hasui, Y. p. 345-368.

Kelsey, D.E., Hand, M., 2011. On ultrahigh temperature crustal metamorphism: Phase equilibria, trace element thermometry, bulk composition, heat sources, timescales and tectonic settings. Geoscience Frontiers, 6, 311-356.

Koester, E, Porcher, C.C., Pimentel, M.M., Fernandes, L.A.D., Vignol-Lelarge, M.L., Oliveira, L.D., Ramos, R.C., 2016. Further evidence of 777 Ma subduction-related continental arc magmatism in Eastern Dom Feliciano Belt, southern Brazil: The Chácara das Pedras Orthogneiss. Journal of South American Earth Sciences, 68, 155-166.

Konopásek, J., Janoušek, V., Oyhantçabal, P., Sláma J ., Ulrich, S., 2018. Did the circum-Rodinia subduction trigger the Neoproterozoic rifting along the Congo–Kalahari Craton margin? International Journal of Earth Sciences, 107(5), 1859-1894.

Lenz, C., 2006. Evolução metamórfica dos metapelitos da Antiforme Serra Dos Pedrosas: condições e idades do metamorfismo. Unpublished MSc thesis. Universidade Federal do Rio Grande do Sul, 128 p. Avaliable at: https://lume.ufrgs.br/handle/10183/8520

Lenz, C., Fernandes, L.A.D., McNaughton, N.J., Porcher, C.C., Masquelin, H., 2011. U–Pb SHRIMP ages for the Cerro Bori orthogneisses, Dom Feliciano Belt in Uruguay: evidences of a ~ 800 Ma magmatic and ~ 650 Ma metamorphic event. Precambrian Research 185, 149–163.

Lenz, C., Porcher, C.C., Fernandes, L.A.D., Masquelin, H., Koester, E., Conceição, R.V., 2013. Geochemistry of the Neoproterozoic (800–767 Ma) Cerro Bori orthogneisses, Dom Feliciano Belt in Uruguay: tectonic evolution of an ancient continental arc. Mineralogy and Petrology 107, 785–806.

Liégeois, J.P., 1998. Preface - Some words on the post-collisional magmatism. Lithos, 45, xvxvii.

Lister, G., Foster, M., 2009. Tectonic mode switches and the nature of orogenesis. Lithos, 113:274-291.

Lyra, D.S., Savian, J.F., Bitencourt, M.F., Trindade, R.I.F., Tomé, C.R., 2018. AMS fabrics and emplacement model of Butia Granite, an Ediacaran

syntectonic peraluminous granite from southernmost Brazil. Journal of South American Earth Sciences, 87, 28-41.

Marques, J.C., Roisenberg, A., Jost, H., Frantz, J.C., Teixeira, R.S., 2003. Geologia e geoquímica das rochas metaultramáficas da Antiforme Capané, Suíte Metamórfica Porongos, RS. Revista Brasileira de Geociências, 33(1), 83-94.

Martil, M. M. D. 2007. Relações de intrusão do Maciço Sienítico Piquiri, RS com suas Encaixantes. Porto Alegre, 63 p. *Monografia de Conclusão de Curso*, Curso de Geologia, Instituto de Geociências, Universidade Federal do Rio Grande do Sul.

Martil, M.M.D., 2016. O magmatismo de arco continental pré-colisional (790 ma) e a reconstituição espaço-temporal do regime transpressivo (650 Ma) no Complexo Várzea do Capivarita, sul da Província Mantiqueira. Unpublished PhD thesis. Universidade Federal do Rio Grande do Sul. Avaliable at: https://www.lume.ufrgs.br/handle/10183/149194

Martil, M.M.D., Bitencourt, M.F., Nardi, L.V.S., 2011. Caracterização estrutural e petrológica do magmatismo pré-colisional do Escudo Sul-rio-grandense: os ortognaisses do Complexo Metamórfico Várzea do Capivarita. Pesquisas em Geociências, 38, 181-201.

Martil, M.M.D., Bitencourt, M.F., Nardi, L.V.S., Koester, E., Pimentel, M.M., 2017. Pre-collisional, Neoproterozoic (ca. 790 Ma) continental arc magmatism in southern Mantiqueira Province, Brazil: geochemical and isotopic constraints from the Várzea do Capivarita Complex. Lithos 274–275:39–52

Masquelin H., Fernandes, L.A.D., Lenz, C., Porcher, C.C., McNaughton, N.J. 2012. The Cerro Olivo Complex: a pre-collisional Neoproterozoic magmatic arc in Eastern Uruguay. International Geology Review, 54, 1161–1183.

Meira, V.T., García-Casco, A., Hyppolito, T., Juliano, C., Schorscher, J.H.D., 2019. Tectono metamorphic evolution of the Central Ribeira Belt, Brazil: a case of late Neoproterozoic intracontinental orogeny and flow of partially molten deep crust during the assembly of West Gondwana. Tectonics, 38(8):3182-3209.

Meira, V.T., García-Casco, A., Juliano, C., Almeida, R.P., Schorscher, J.H.D., 2015. The role of intracontinental deformation in supercontinent assembly: insights from the Ribeira Belt, Southeastern Brazil (Neoproterozoic West Gondwana). Terra Nova, 27, 206-217.

Mezger, J.E., Chacko, T., Erdmer, P., 2008. Metamorphism at a late Mesozoic accretionary margin: a study from the Coast Belt of the North American Cordillera. Journal of Metamorphic Geology, 19:121-137.

Nardi, L.V.S., Plá-Cid, J., Bitencourt, M.F., Stabel, L.Z., 2008. Geochemistry and petrogenesis of post-collisional ultrapotassic syenites and granites from southernmost Brazil: the Piquiri Syenite Massif. Anais da Academia Brasileira de Ciências 80(2): 353-371.

Niessing, M., 2008. Geology and stratigraphic definition of the Butiá Granite: a sillimanite-bearing syntectonic leucogranite from the Sul-rio-grandense Shield. Unpublished MSc thesis. Technischen Universität München.

Oliveira, C.H.E., Chemale Jr., F., Jelinek, A.R., Bicca, M.M., Philipp, R.P., 2014. U–Pb and Lu–Hf isotopes applied to the evolution of the late topost-orogenic transtensional basins of the dom feliciano belt, Brazil. Precambrian Research, 246:240–255.

Oriolo, S., Oyhantçabal, P., Wemmer, K., Basei, M. A. S., Benowitz, J., Pfänder, J., Hannich, F., Siegesmund, S., 2016b. Timing of deformation in the Sarandí del Yí Shear Zone, Uruguay: Implications for the amalgamation of western Gondwana during the Neoproterozoic Brasiliano-Pan-African Orogeny, Tectonics, 35, doi:10.1002/2015TC004052.

Oriolo, S., Oyhantçabal, P., Wemmer, K., Heidelbach, F., Pfänder, J., Basei, M.A.S., Hueck, M., Hannich, F., Sperner, B., Siegesmund, S., 2016a. Shear zone evolution and timing of deformation in the Neoproterozoic transpressional Dom Feliciano Belt, Uruguay. Journal of Structural Geology, 92:59-78.

Oriolo S., Oyhantçabal P., Wemmer K., Siegesmund S., 2017. Contemporaneous assembly of Western Gondwana and final Rodinia break-up: Implications for the supercontinent cycle. Geoscience Frontiers, 8, 1431-1445.

Oyhantçabal, P., Siegesmund, S., Wemmer, K., 2011. The Río de la Plata Craton: a review of units, boundaries, ages and isotopic signature. International Journal of Earth Sciences 100, 201-220.

Oyhantçabal, P., Siegesmund, S., Wemmer, K., Presnyakov, S., Layer, P., 2009. Geochronological constraints on the evolution of the southern Dom Feliciano Belt (Uruguay). Journal of the Geological Society of London 166, 1075-1084.

Padilha, D.F., Bitencourt, M.F., Nardi, L.V.S., Forisbal, L.M., Reis, C. Geraldes, M., Almeida, B.S. 2019. Sources and settings of Ediacaran post-collisional syenite-monzonite-diorite shoshonitic magmatism from southernmost Brazil. Lithos, 344-345, 482-503.

Paim, P.S.G., Chemale Jr., F., Wildner, W., 2014. Estágios evolutivos da Bacia do Camaquã (RS). Ciência e Natura, Santa Maria, v. 36, p. 183–193.

Passarelli, C.R., Basei, M.A.S., Wemmer, K., Siga Jr., O., Oyhantçabal, P., 2011. Major shear zones of southern Brazil and Uruguay: escape tectonics in the eastern border of Rio de La plata and Paranapanema cratons during the Western Gondwana amalgamation. International Journal of Earth Sciences, 100, 391–414.

Percival, J.J., Konopásek, J., Eiesland, R., Sláma, J., Campos, R.S., Battisti, M.A., Bitencourt, M.F., 2021. Pre-orogenic connection of the foreland domains of the Kaoko-Dom Feliciano-Gariep orogenic system. Precambrian Research, 354, 106060.

Pertille J., Hartmann L.A., Philipp R.P., Petry T.S., Lana C.C. 2015. Origin of the Ediacaran Porongos Group, Dom Feliciano Belt, southern Brazilian Shield, with emphasis on whole rock and detrital zircon geochemistry and U-Pb, Lu-Hf isotopes. Journal of South American Earth Sciences, 64:69-93.

Picada, R.S., 1971. Ensaio sobre a tectônica do Escudo Sul-riograndense: caracterização dos sistemas de falhas. Anais do XXV Congresso Brasileiro de Geologia. Porto Alegre, Sociedade Brasileira de Geologia. p. 167-191.

Philipp, R.P., Bom, F.M., Pimentel, M.M., Junges, S.L., Zvirtes, G., 2016. SHRIMP U-Pb age and high temperature conditions of the collisional metamorphism in the Varzea do Capivarita Complex: implications for the origin of Pelotas Batholith, Dom Feliciano Belt, southern Brazil. Journal of South American Earth Sciences 66,196–207.

Philipp, R.P., Pimentel, M.M., Basei, M.A.S., 2018. The Tectonic Evolution of the São Gabriel Terrane, Dom Feliciano Belt, Southern Brazil: The Closure of the Charrua Ocean. *in:* S. Siegesmund et al. (eds.), Geology of Southwest Gondwana, Regional Geology Reviews, 243-265.

Philipp, R.P., Machado, R., Nardi, L.V.S., Lafon, J.M., 2002. O Magmatismo Granítico Neoproterozóico do Batólito Pelotas no sul do Brasil: Novos dados e revisão da Geocronologia regional. Brazilian Journal of Geology 32, 277-290

Philipp, R.P., Machado, R., 2005. The late Neoproterozoic granitoid magmatism of the Pelotas Batholith, southern Brazil. Journal of South American Earth Sciences 19, 461-478.

Philipp, R.P., Massonne, H.J., Campos, R. 2013. Peraluminous leucogranites of the Cordilheira Suite: a record of Neoproterozoic collision and the generation of the Pelotas Batholith, Dom Feliciano Belt, Southern Brazil. Journal of South American Earth Sciences, 43, 8-24.

Porcher, C.A., Lopes, R.D.C., 2000. Programa Levantamentos Geológicos Básicos do Brasil. Mapa Geologico da Folha Cachoeira do Sul, Folha SH.22-YA. Escala 1: 25.000. Serviço Geológico do Brasil (CPRM), Brasília.

Ramgrab, G.E., Wildner, W., Camozzato, E., 1996. Programa de Levantamentos Geológicos Básicos do Brasil, Mapa Geologico da Folha Porto Alegre SH. 22-YB. Escala 1:25.000. Serviço Geologico do Brasil (CPRM), Brasília, p. 144.

Ramos, R.C., Koester, E., Triboli, D.V., Porcher, C.C., Gezatt, J.N., Silveira, R.L., 2018. Insights on the evolution of the Arroio Grande Ophiolite (Dom Feliciano Belt, Brazil) from Rb-Sr and SHRIMP U-Pb isotopic geochemistry. Journal of South American Earth Sciences, 86:38-53.

Rivera, C.B., 2019. Construção do Maciço Sienítico Piquiri (609 a 583 ma) por colocação sucessiva de pulsos de magma ultrapotássico e shoshonítico sob extensão no Escudo sul-rio-grandense. PhD thesis. Universidade Federal do Rio Grande do Sul. Porto Alegre, Brazil.

Saalmann, K., Gerdes, A., Lahaye, Y., Hartmann, L.A., Remus, M.V.D., Läufer, A., 2011. Multiple accretion at the eastern margin of the Rio de la Plata craton: the prolonged Brasiliano orogeny in southernmost Brazil. International Journal of Earth Sciences, 100, 355-378.

Saalmann, K., Remus, M.V.D., Hartmann, L.A., 2006. Structural evolution and tectonic setting of the Porongos Belt, southern Brazil. Geological Magazine, 143, 59-88.

Sbaraini, S., Raposo, M.I.B., Bitencourt, M.F., Tomé, C.R., 2020. Magnetic fabrics of the neoproterozoic piquiri syenite massif (Southernmost Brazil): Implications for 3D geometry and emplacement. Journal of Geodynamics, 134, 101691.

Sengör, A.M.C, Dewey, J.F., 1990. Terranology: Vice or Virtue? *in:* Dewey, J.F., Gass, I.G., Curry, G.B., Harris, N.B.W, Sengör, A.M.C., eds. Allochtonous terranes. Cambridge, Cambridge University Press. p. 23-29.

Shroder, J., 2014. Air and Space Technology in Resource Delineation: Peace and War. *in:* Natural Resources in Afghanistan: : Geographic and Geologic Perspectives on Centuries of Conflict. Elsevier, p.381-406. http://dx.doi.org/10.1016/B978-0-12-800135-6.00013-1

Silva, L.C., Hartmann, L.A., McNaughton, N.J., Fletcher, I.R., 1999. SHRIMP U/Pb Zircon dating of Neoproterozoic granitic magmatism and collision in the Pelotas Batholith, Southernmost Brazil. International Geology Review, 41, 531–551.

Stabel, L.S., Nardi, L.V.S., Plá Cid, J., 2001. Química mineral e evolução petrológica do Sienito Piquiri: magmatismo shoshonítico, neoproterozóico, pós-colisional no sul do Brasil. Revista Brasileira de Geociências, 31(2):211-222.

Tajcmanová, L., Konopásek J., Connoly, J.A.D., 2007. Diffusion-controlled development of silica-undersaturated domains in felsic granulites of the Bohemian Massif (Variscan belt of Central Europe). Contributions to Mineralogy and Petrology 153: 237-250.

Tajcmanová, L., Connolly, J.A.D.,Cesare, B., 2009. A thermodynamic model for titanium and ferric iron solution in biotite. Journal of Metamorphic Geology 27,153-64.

Tambara, GB, Koester, E, Ramos, RC, Porcher, CC, Vieira, DT, Fernandes, LAD, Lenz, C. Geoquímica e geocronologia dos Gnaisses Piratini: magmatismo cálcio-alcalino médio a alto-K de 784 Ma (U-Pb SHRIMP) no SE do Cinturão Dom Feliciano (RS, Brasil). Pesquisas em Geociências, v. 46 (2019), n. 2:e0769. doi.org/10.22456/1807-9806.95466

Thompson, A.B., Schulmann, K., Jezek, J., Tolar, V., 2001. Thermally softened continental extensional zones (arcs and rifts) as precursors to thickened orogenic belts. Tectonophysics, 332:115-141.

Vieira, D.T., Koester, E., Ramos, R.C., Porcher, C.C., Fernandes, L.A.D., SHRIMP U-Pb zircon ages for the synkinematic magmatism in the Dorsal de Canguçu Transcurrent Shear Zone, Dom Feliciano Belt (Brazil): Tectonic implications. Journal of South American Earth Sciences, 100, 102603.

UFRGS, 2008. Mapeamento Geológico 1:25 000 de parte das folhas Passo das Canas SH-22-Y-A-III-4 (MI2984/4) e Capané SH 22-Y-A-III-3 (MI2984/3), RS. Instituto de Geociências, Universidade Federal do Rio Grande do Sul, Porto Alegre.

UFRGS, 2009. Mapeamento Geológico 1:25 000 de parte da Folha Passo das Canas SH-22-Y-A-III-4 (MI2984/4), RS. Instituto de Geociências, Universidade Federal do Rio Grande do Sul, Porto Alegre.

UFRGS, 2010. Mapeamento Geológico 1:25 000 de parte das folhas Encruzilhada SH-22-Y-A-VI-2 (MI2997/2) e Passo das Canas SH22-Y-A-III-4 (MI2984/4), RS. Instituto de Geociências, Universidade Federal do Rio Grande do Sul, Porto Alegre.

UFRGS, 2011. Mapeamento Geológico 1:25 000 de parte da folha Várzea do Capivarita SH-22-Y-B-I-4 (MI2985/2), RS. Instituto de Geociências, Universidade Federal do Rio Grande do Sul, Porto Alegre.

Weinberg, R.F., 2016. Himalayan leucogranites and migmatites: nature, timing and duration of anatexis. Journal of Metamorphic Geology, 34(8):821-843.

White, R.W., Powell, R.,Holland, T.J.B., 2001. Calculation of partial melting equilibria in the system Na2O-CaO-K2O-FeO-MgO-Al2O3-SiO2-H2O (NCKFMASH). Journal of Metamorphic Geology 19, 139-53.

Will, T.M., Gaucher, C., Ling, X.-H., Li, X.-H., Li, Q.-L., Frimmel, H.E. Neoproterozoic magmatic and metamorphic events in the Cuchilla Dionisio Terrane, Uruguay, and possible correlations across the South Atlantic. Precambrian Research, 320, 303-322.

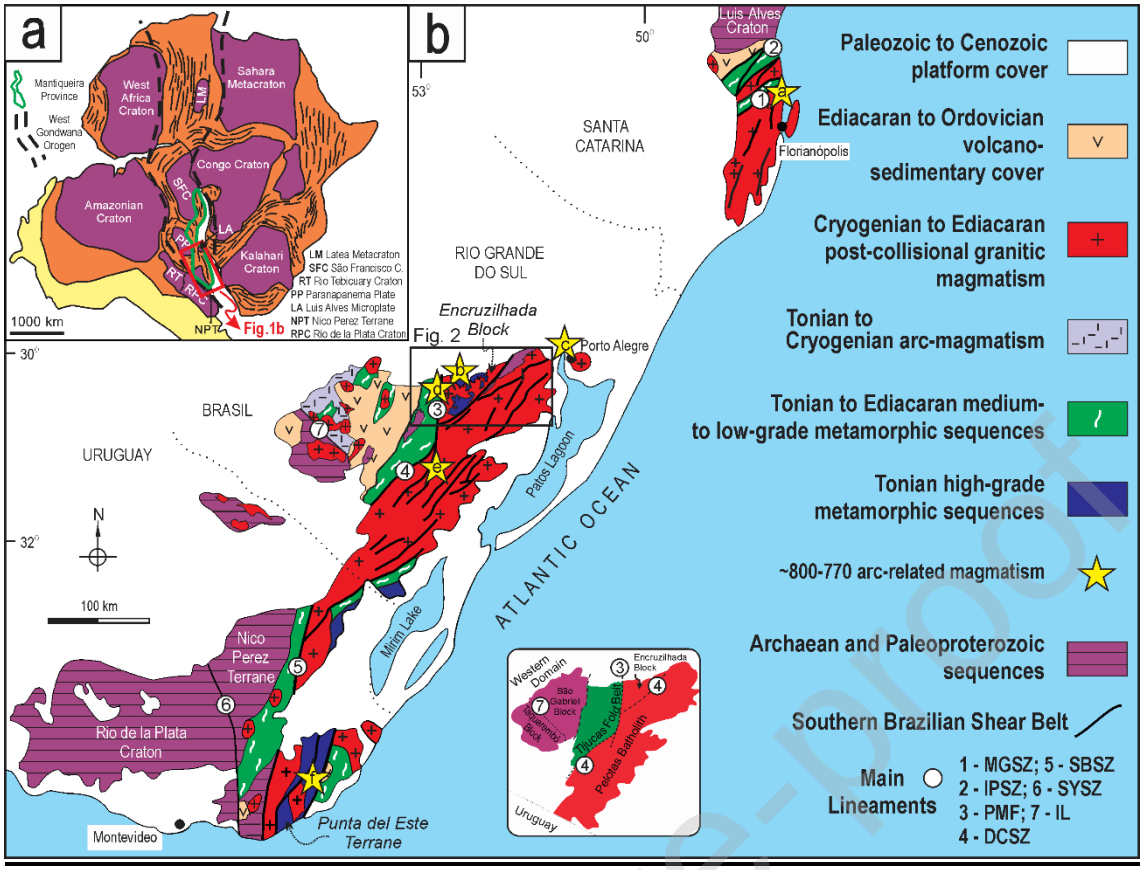

Figure 1 – (a) Geotectonic sketch of Western Gondwana (modified from Oriolo et al., 2017; Dragone et al., 2017; Will et al., 2019). (b) Geotectonic map of Dom Feliciano Belt and surrounding cratonic blocks (modified from Bitencourt and Nardi, 2000, Ramos et al., 2018; Will et al., 2019). Area of Fig. 2 indicated. MGSZ – Major Gercino Shear Zone; IPSZ – Itajaí-Perimbó Shear Zone; PMF – Passo do Marinheiro Fault; DCSZ – Dorsal de Canguçu Shear Zone; SBSZ – Sierra Ballena Shear Zone; SYSZ – Sarandi del Yi Shear Zone; IL – Ibaré Lineament. Tonian arc-related magmatism: a – De Toni et al., 2020a; b – Martil et al., 2017; c – Koester et al., 2016; d – Battisti et al., 2018; e – Silva et al., 1999; Tambara et al., 2019; e – Lenz et al., 2011; 2013. The inset features a simplified subdivision of the shield areas in Rio Grande do Sul and their main lineament boundaries. [2-column]

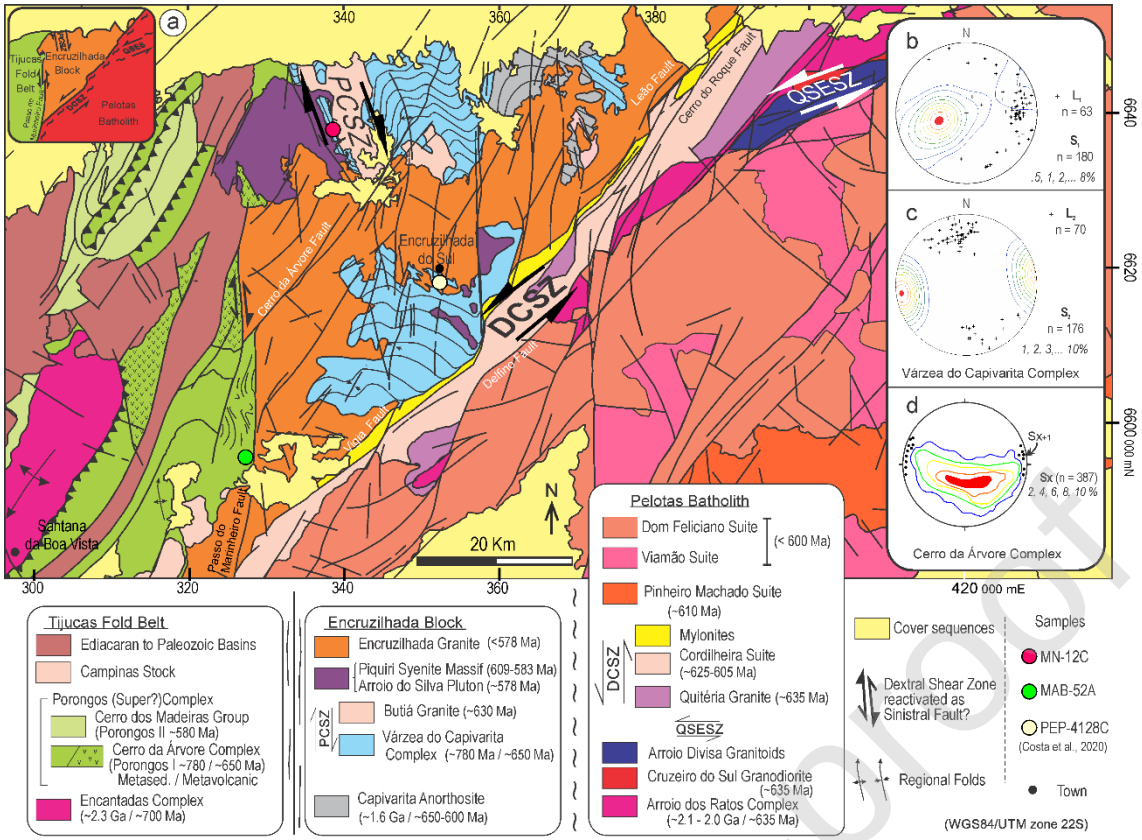

Figure 2 – (a) Geological map of the Encruzilhada Block and adjacent regions (compiled from Picada, 1971; Jost and Bitencourt, 1980; Ramgrab et al., 1996; Porcher and Lopes, 2000; Philipp et al., 2002; UFRGS, 2008, 2009, 2010, 2011; Gregory et al., 2015; Martil, 2016; Höfig et al., 2017). Major faults and shear zones: DCSZ – Dorsal de Canguçu Shear Zone; QSESZ – Quitéria-Serra do Erval Shear Zone; PCSZ – Passo das Canas Shear Zone. Inset shows the location of the Encruzilhada Block and boundaries of neighbouring tectonic domains. (b) Structural data with contoured main foliation and lineation from Várzea do Capivarita Complex D_1 and (c) D_2 (both from Martil et al., 2017). (d) Structural data with contoured main foliation S_x and transposition foliation S_{x+1} from Cerro da Árvore Complex (from Jost and Bitencourt, 1980). [2-column]

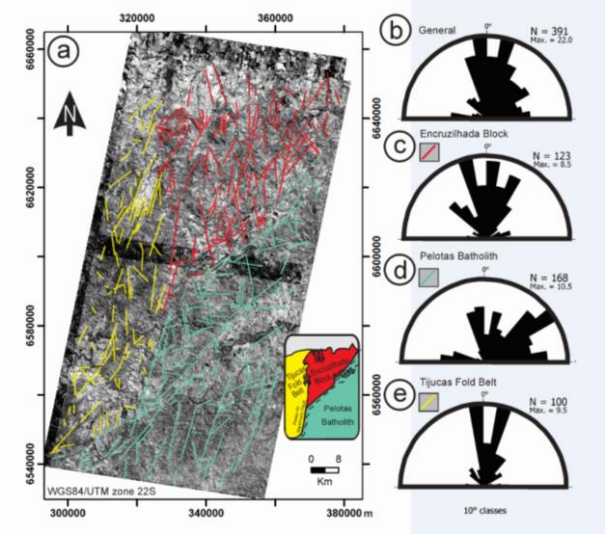

Figure 3 – Satellite image analysis. (a) ASTER images used for creation of digital elevation model and lineament tracing; inset illustrates tectonic domains. Frequency rose diagrams representative of the general map (b), Encruzilhada Block (c), Major Gercino Shear Zone (d) and Tijucas Fold Belt (e). [2-column]

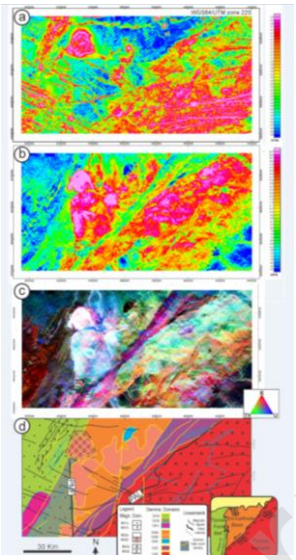

Figure 4 – Aerogeophysical maps for the Encruzilhada Block and surrounding areas. All maps cover the same area as the geological map of figure 2. (a) Analytic signal amplitude of the aeromagnetic anomaly map; (b) Aerogammaspectrometric total count map; (c) Aerogammaspectrometric ternary (K-Th-U – RGB) composition map; (d) Interpretative sketch containing geophysical lineaments and domains made from the three previous maps. Legend is colored for gammaspectrometric domains (Gd) and hatched for magnetometric domains (Md). [2-column]

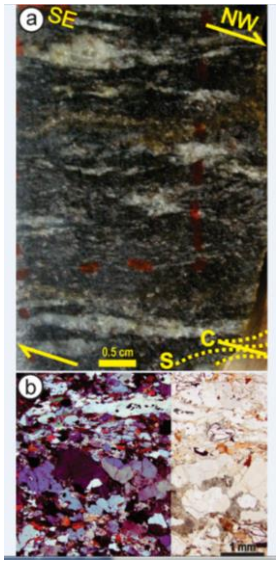

Figure 5 – Petrographic features of Várzea do Capivarita Complex metapelite sample MN-12C. (a) Handsample overview (XZ plane). Metamorphic fabric is enhanced by leucocratic bands with igneous texture, interpreted as leucosome. Leucosome is distributed into S-C fabrics indicative of top-to-the-NW shear sense. (b) Microscopic overview under crossed (left) and plane polarizers (right) featuring textural and compositional heterogeneity of the main banding. [1-column]

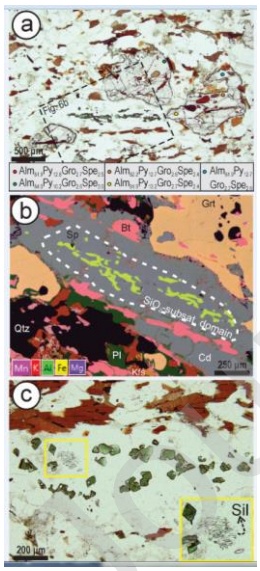

Figure 6 – Melanosome aspects of Várzea do Capivarita Complex metapelite sample MN-12C. (a) Garnet and cordierite porphyroblasts with round inclusions of biotite and quartz, and subhedral, well-aligned green spinel. Dashed rectangle indicates the area of compositional map of figure 6b. Coloured dots mark microprobe analysed points, with compositions indicated in the legend.

Plane-polarized light. (b) SEM-EDS compositional map from SiO_2-subsaturated domain. The main minerals are represented by different colors and labelled. White dashed line outlines the area for which the system composition was estimated. Colour code is indicated. (c) Cordierite porphyroblast including subhedral spinel and fine-grained sillimanite aggregate (inset). Plane-polarized light. [1-column]

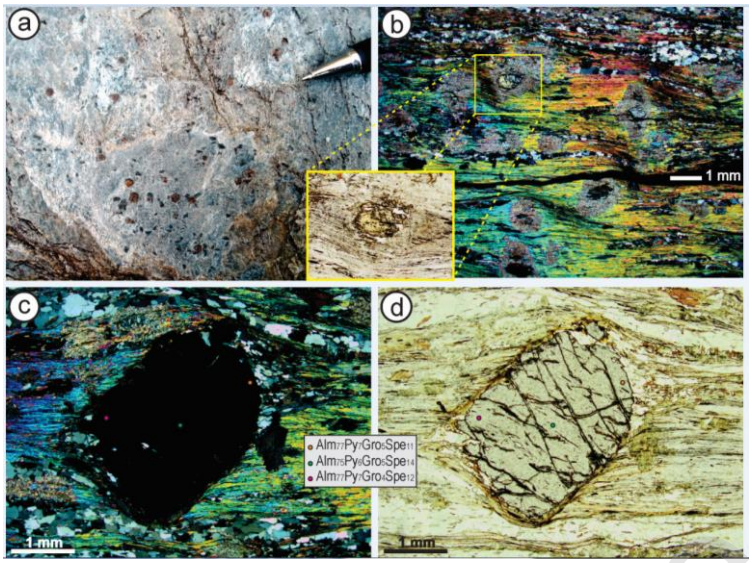

Figure 7 – Petrographic features of Cerro da Árvore Complex garnet-staurolite-mica schist, smaple MAB-52A. (a) Mesoscopic aspect in XY view at outcrop subhorizontal surface, with garnet (red) and staurolite (black) mm-size porphyroblasts in a muscovite-rich layer. (b) Microscopic overview of a staurolite-rich layer under cross-polarized light. Inset for partially replaced staurolite porphyroblast with characteristic golden yellow pleochroism, at plane-polarized light. (c) and (d) Synkinematic garnet porphyroblast under cross-polarized and plane-polarized light, respectively. Microprobe point analyses are marked by coloured spots and the results are presented as calculated end-members. Late- to post-kinematic chlorite occurs as up to 1 mm-large radial aggregates that overgrow the main schistosity, as observed on the right-hand side of the garnet porphyroblast. [2-column]

Figure 8 – Post-kynematic andalusite growth on Cerro da Árvore Complex garnet-staurolite mica schist: (a) Cm-size andalusite (prismatic section) formed along a fracture in metapelite. (b) Andalusite (basal section) microscopic overview under cross-polarized light (photomicrograph mosaic). Staurolite inclusions are preserved from replacement. [1-column]

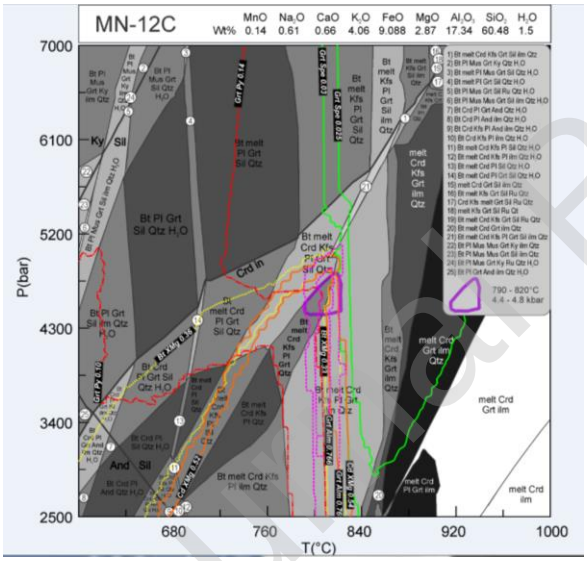

Figure 9 – Várzea do Capivarita Complex migmatitic metapelite (MN-12C) pseudosection. System chemical composition is shown in the upper bar, main mineral stability fields are labeled, and the observed assemblage (Bt + melt + Crd + Kfs + Pl + Grt + Qtz) is in bold letters. Smaller fields are labeled according to the displayed numerical legend. Coloured isopleths define an overlapping area correspondent to 790 – 820°C and 4.4 – 4.8 kbar. Isopleths: red for garnet pyrope 0.10 – 0.14; pink for garnet almandine 0.76 – 0.766; orange for cordierite X_{Mg} 0.52 – 0.54; and yellow for biotite X_{Mg} 0.33 – 0.36. The curves for

cordierite-in and the aluminum-silicate pseudomorph curves are also shown. [1.5-column]

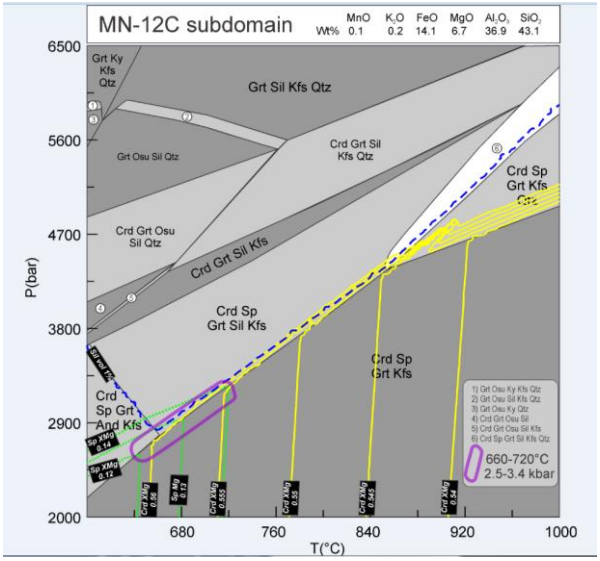

Figure 10 – Várzea do Capivarita Complex migmatitic metapelite (MN-12C) SiO_2-subsaturated domain pseudosection. System chemical composition, taken from the compositional map of Fig. 6b, is shown in the upper bar. Main mineral stability fields are labeled and smaller fields are labeled according to the displayed numerical legend. The observed mineral assemblage (Crd+Sp+Grt+Sp+Kfs) defines a wide field. Coloured isopleths and the additional curve for sillimanite modal 1 % (blue dashed line) define a very small area, indicated by the purple ellipse and correspondent to 660 – 720°C and 2.5 – 3.4 kbar. Isopleths: green for spinel X_{Mg} 0.12 – 0.14; yellow for cordierite X_{Mg} 0.54 – 0.56. [1.5-column]

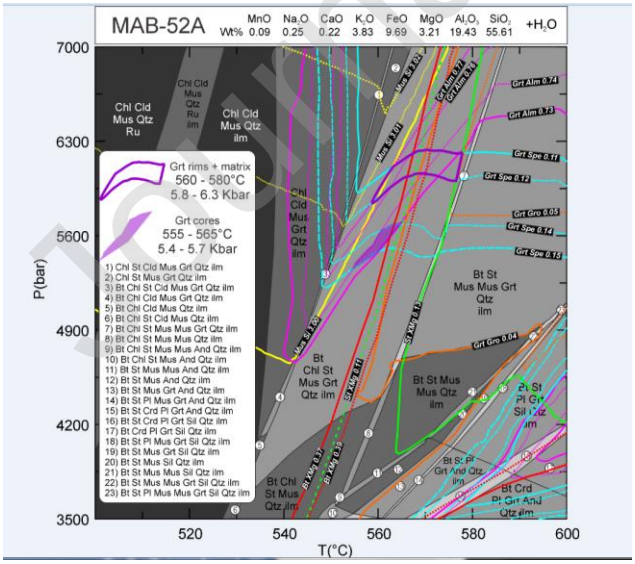

Figure 11 – Cerro da Árvore Complex staurolite-garnet-quartz-muscovite schist (MAB-52A) pseudosection. The system is water-saturated and the composition is shown in the upper bar. Main mineral stability fields are labeled and smaller fields are labeled according to the numerical legend. Observed mineral assemblage (Bt+Chl+St+Mus+Grt+Qtz+ilm) defines the central polygon. Crossing coloured isopleths define two distinct metamorphic conditions. Garnet cores (smaller, purple area), with spessartine 0.14 – 0.15 and almandine 0.73 – 0.74 records 555 – 565°C and 5.4 – 5.7 kbar early growth. Garnet rims with spessartine 0.11 – 0.12, almandine 0.73 – 0.77 and grossular 0.04 – 0.05, together with staurolite X_{Mg} 0.11 – 0.13, biotite X_{Mg} 0.37 – 0.39 and muscovite Si apfu 3.00 from the matrix, define a wider polygon (thicker purple contour) which points to 560 – 580°C and 5.8 – 6.3 kbar as peak metamorphic conditions. [1.5-column]

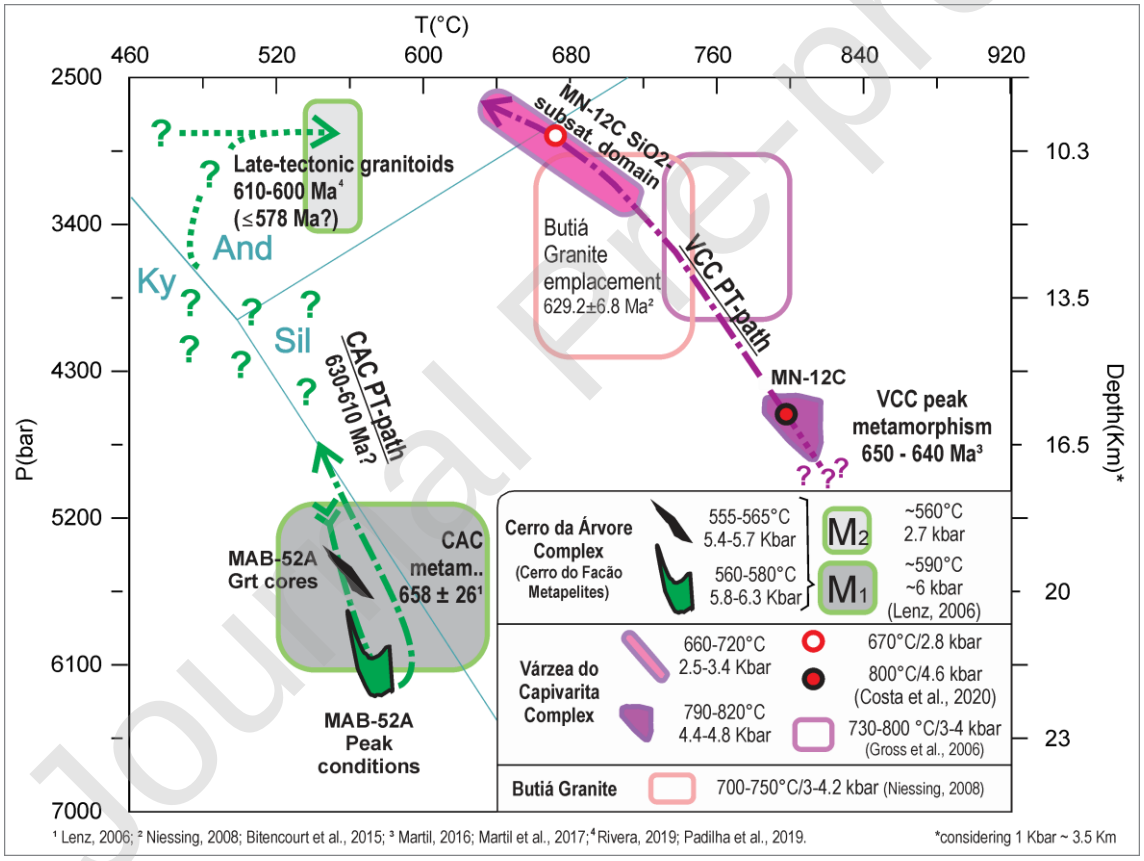

Figure 12 – Summarizing figure with all PT estimatives for Várzea do Capivarita (VCC) and Cerro da Árvore (CAC) complexes from this work integrated with previously published results from Gross et al. (2006), Lenz (2006), Niessing (2008) and Costa et al. (2020), and ages from Martil (2016), Bitencourt et al.

(2015, 2016), Rivera (2019) and Padilha et al. (2019). PT-paths are traced with dashed lines. [1.5-column]

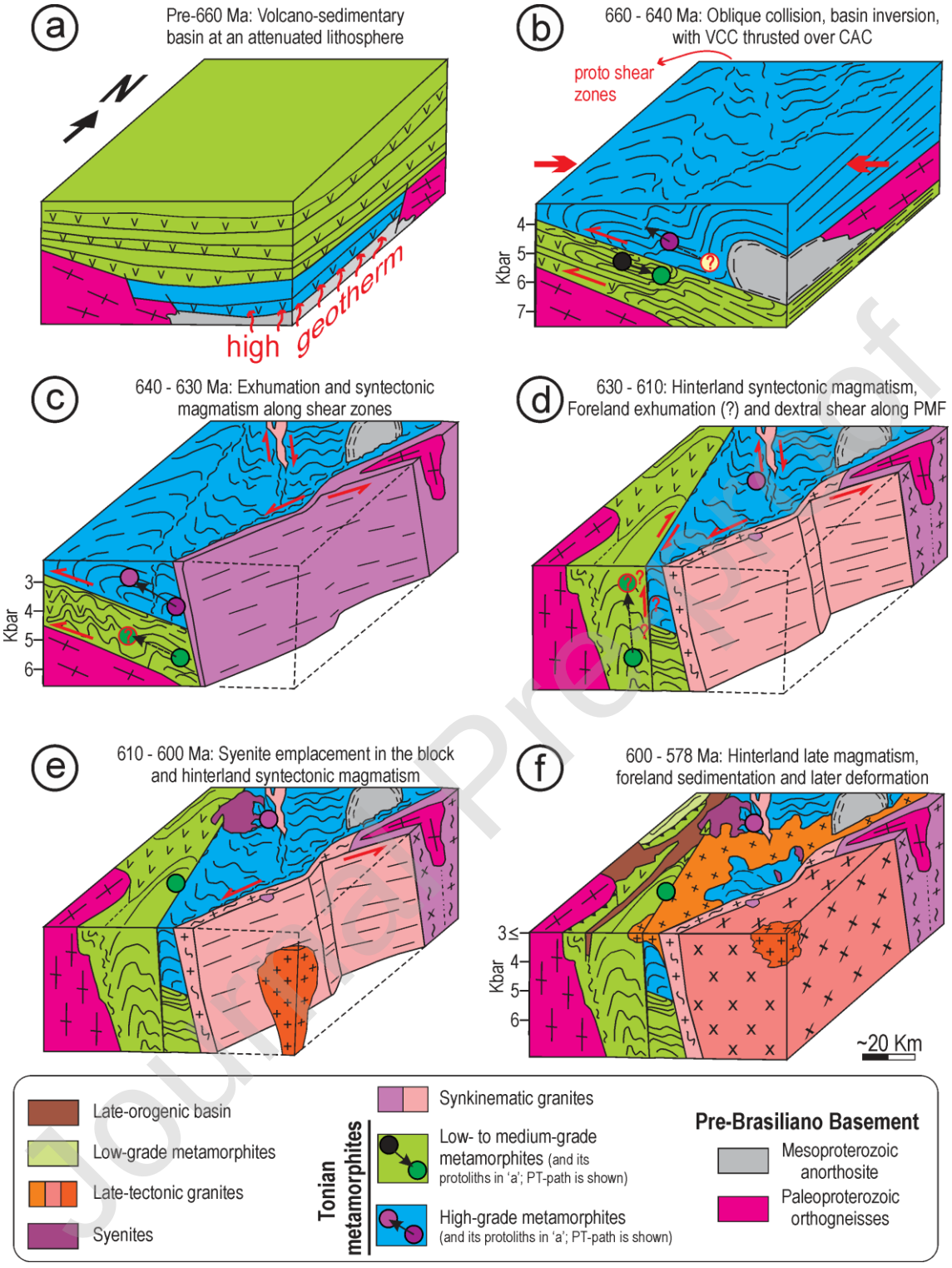

Figure 13 – Model for the autochtonous origin of the Encruzilhada Block. (a) Pre-660 Ma: precursor volcano-sedimentary basin over an attenuated lithosphere, with high geothermal gradient; (b) 660-640 Ma: basin inversion during oblique collision, with Várzea do Capivarita Complex thrusted over Cerro

da Árvore Complex; (c) 640-630 Ma: exhumation while active shear zones focused magmatism; (d) after 630 Ma: foreland exhumation (?) due to Passo do Marinheiro Fault displacement, while syntectonic magmatism emplaced along hinterland active shear zones; (e) 610-600 Ma: Piquiri Syenite Massif emplacement across the Passo do Marinheiro Fault; (f) 600-578 Ma: Encruzilhada Granite emplacement blurred the western boundary of the block, while sedimentation and late-deformation occurred in the foreland, which gives the present map configuration (surface based on Fig. 2a). Abbreviations as in figures 4 and 12. [2-column]

Table 1 – VCC metapelitic paragneiss (MN12C) mineral chemistry.

Mineral	Cordierite						Spinel			
Site	1-2 c	1-2 c	1-2 c	1-2 m	4 c	4 m	Site	01-2 i	4 i	4 i
Na2O	0.31	0.30	0.34	0.37	0.23	0.31	SiO2	0.01	0.03	0.01
SiO2	47.72	48.07	48.03	47.78	48.11	48.12	MgO	2.68	2.67	2.57
MgO	7.17	7.09	6.87	6.94	7.29	7.04	Al2O3	55.9	55.41	56.35
Al2O3	32.52	32.37	32.55	32.58	32.50	32.48	CaO	0	0.01	0
K2O	0.00	0.01	0.00	0.01	0.01	0.00	TiO2	0.03	0.08	0.07
CaO	0.03	0.02	0.02	0.03	0.02	0.03	Cr2O3	0.1	0.1	0.14
TiO2	0.01	0.01	0.01	0.02	0.01	0.02	FeO	32.19	32.58	33.05
FeO	10.15	10.22	10.08	10.53	9.88	9.94	Fe2O3	2.64	2.99	2.03
MnO	0.11	0.11	0.13	0.13	0.10	0.12	MnO	0.11	0.14	0.11
Cr2O3	0.00	0.00	0.00	0.01	0.00	0.00	ZnO	4.12	3.59	3.52
ZnO	0.03	0.01	0.00	0.00	0.00	0.00	Total	97.77	97.60	97.84
Total	98.05	98.20	98.03	98.38	98.17	98.06				
							No. Cations in Formula (on the basis of 32 O)			
No. Cations in Formula (on the basis of 18 O)							Si	0.00	0.01	0.00
Na	0.063	0.061	0.069	0.075	0.046	0.063	Mg	0.95	0.95	0.91
Si	4.977	5.004	5.004	4.975	5.001	5.009	Al	15.57	15.49	15.63
Mg	1.115	1.100	1.067	1.077	1.129	1.092	Ca	0.00	0.00	0.00
Al	3.998	3.972	3.998	3.999	3.982	3.985	Ti	0.01	0.01	0.01
K	0.000	0.001	0.000	0.001	0.001	0.000	Cr	0.02	0.02	0.03
Ca	0.003	0.002	0.002	0.003	0.002	0.003	Fe(ii)	6.33	6.43	6.48
Ti	0.001	0.001	0.001	0.002	0.001	0.002	Fe(iii)	0.47	0.53	0.36
Fe	0.885	0.890	0.878	0.917	0.859	0.865	Mn	0.02	0.03	0.02
Mn	0.010	0.010	0.011	0.011	0.009	0.011	Zn	0.72	0.63	0.61
Cr	0.000	0.000	0.000	0.001	0.000	0.000	Total (S)	24.09	24.10	24.05
Zn	0.002	0.001	0.000	0.000	0.000	0.000				
Total	11.054	11.040	11.030	11.061	11.031	11.029	XFe	87.9	88.1	88.4
XMg	55.735	55.288	54.850	54.018	56.807	55.799	XMg	0.12	0.12	0.12

Site obs.: c = center; m = margin; s = small; i = inclusion; a = in aggregate; l = in leucossome.

Table 1 (cont.)

Garnet										
Site	01-2 c	01-2 m	01-2 m	01-2 c	01-2 m	03 c	03 m	03 s	03 s	03 s
SiO2	37.66	36.93	36.96	37.12	37.49	36.95	37.10	37.40	37.26	36.97
MgO	3.14	2.53	3.12	3.14	3.30	3.04	3.09	3.12	2.72	3.25
Al2O3	21.26	21.23	21.51	21.51	21.33	21.24	21.08	21.36	21.18	21.40
CaO	0.91	0.91	0.93	0.91	0.95	0.92	0.94	0.92	0.92	0.94
TiO2	0.03	0.04	0.03	0.06	0.03	0.04	0.03	0.03	0.04	0.05
FeO	35.76	36.90	35.81	36.09	36.27	36.13	36.31	36.51	36.90	35.77
MnO	1.09	1.33	1.14	1.03	1.06	1.46	1.14	1.22	1.18	1.06
Total	99.85	99.87	99.50	99.85	100.43	99.79	99.70	100.57	100.21	99.45
No. Cations in Formula (on the basis of 24 O)										
Si	6.05	5.98	5.97	5.98	6.00	5.97	6.00	5.99	6.00	5.97
Mg	0.75	0.61	0.75	0.75	0.79	0.73	0.74	0.74	0.65	0.78
Al	4.02	4.05	4.10	4.08	4.03	4.05	4.02	4.03	4.02	4.08
Ca	0.16	0.16	0.16	0.16	0.16	0.16	0.16	0.16	0.16	0.16
Ti	0.00	0.00	0.00	0.01	0.00	0.00	0.00	0.00	0.00	0.01
Fe	4.80	5.00	4.84	4.86	4.86	4.88	4.91	4.89	4.97	4.83
Mn	0.15	0.18	0.16	0.14	0.14	0.20	0.16	0.17	0.16	0.15
Total	15.94	15.99	15.98	15.98	15.98	16.00	15.99	15.99	15.98	15.98
End-member calculations										
PY	12.83	10.27	12.72	12.75	13.24	12.26	12.47	12.50	10.99	13.21
ALM	81.97	84.01	81.91	82.22	81.61	81.73	82.19	82.07	83.63	81.59
GRO	2.67	2.65	2.73	2.66	2.74	2.67	2.73	2.65	2.67	2.75
SP	2.53	3.07	2.64	2.38	2.42	3.35	2.61	2.78	2.71	2.45
XMg	0.14	0.11	0.13	0.13	0.14	0.13	0.13	0.13	0.12	0.14

Table 1 (cont.)

Micas										
Site	01-2	01-2	01-2	01-2 i	1-1 m	01 a	01 m	01 m	03 l	04 a
Na2O	0.14	0.13	0.12	0.15	0.12	0.12	0.12	0.11	0.08	0.12
SiO2	35.25	35.99	35.89	35.40	35.64	35.95	35.76	35.43	36.01	35.76
MgO	6.30	6.20	6.26	6.57	6.31	6.12	6.67	6.86	6.87	6.74
Al2O3	17.78	17.46	18.04	17.33	17.93	17.64	17.52	18.03	17.27	18.03
K2O	9.23	9.38	9.37	9.25	9.14	9.30	9.36	9.35	9.54	9.41
CaO	0.00	0.00	0.00	0.00	0.00	0.00	0.00	0.00	0.00	0.00
TiO2	4.19	4.08	3.83	4.34	3.39	4.15	4.20	3.41	4.08	3.99
FeO	22.18	22.68	22.04	22.17	22.40	22.73	21.72	22.56	21.36	21.67
MnO	0.08	0.09	0.06	0.02	0.08	0.04	0.09	0.02	0.03	0.05
Total	95.16	96.00	95.61	95.24	95.01	96.06	95.45	95.78	95.24	95.75
No. Cations in Formula (on the basis of 22 O)										
Na	0.04	0.04	0.04	0.04	0.04	0.04	0.04	0.03	0.02	0.04
Si	5.45	5.52	5.51	5.47	5.51	5.51	5.50	5.45	5.54	5.47
Mg	1.45	1.42	1.43	1.51	1.45	1.40	1.53	1.57	1.58	1.54
Al	3.24	3.16	3.26	3.16	3.27	3.19	3.18	3.27	3.13	3.25
K	1.82	1.84	1.83	1.82	1.80	1.82	1.84	1.83	1.87	1.84
Ca	0.00	0.00	0.00	0.00	0.00	0.00	0.00	0.00	0.00	0.00
Ti	0.49	0.47	0.44	0.50	0.39	0.48	0.49	0.39	0.47	0.46
Fe	2.87	2.91	2.83	2.86	2.90	2.91	2.79	2.90	2.75	2.77
Mn	0.01	0.01	0.01	0.00	0.01	0.01	0.01	0.00	0.00	0.01
Total	15.37	15.37	15.35	15.38	15.38	15.35	15.36	15.46	15.37	15.38
XMg	33.61	32.76	33.61	34.56	33.43	32.43	35.37	35.15	36.44	35.67

Table 2 - Cerro da Árvore Complex grt-st-mica schist mineral chemistry

Mineral	Staurolite										
SiO2	27.12	27.45	27.76	26.68	27.30	26.52	27.29	27.39	27.09	26.65	27.38
MgO	1.04	0.96	1.03	1.04	0.89	1.04	1	0.84	0.81	1.02	1.08
Al2O3	54.81	55.10	54.36	55.30	55.19	56.22	55.23	55.69	55.66	56.37	55.43
CaO	0.01	0.00	0.01	0.01	0.00	0	0	0.00	0.00	0.01	0
FeO	12.96	12.65	12.50	13.22	12.28	13.32	13.14	12.15	11.96	12.95	13.05
TiO2	0.70	0.59	0.71	0.37	0.43	0.38	0.88	0.45	0.38	0.33	0.48
MnO	0.27	0.21	0.26	0.22	0.27	0.21	0.25	0.24	0.28	0.27	0.25
ZnO	1.29	1.54	1.53	1.42	2.25	1.32	1.43	2.19	2.03	1.44	1.45
Total	98.20	98.51	98.15	98.25	98.62	99.02	99.23	98.97	98.2	99.05	99.12
No. Cations in Formula (on the basis of 46 O)											
Si	7.53	7.58	7.69	7.41	7.55	7.31	7.50	7.54	7.50	7.34	7.53
Mg	0.43	0.40	0.43	0.43	0.37	0.43	0.41	0.34	0.33	0.42	0.44
Al	17.93	17.94	17.75	18.11	17.99	18.27	17.90	18.06	18.17	18.29	17.97
Ca	0.00	0.00	0.00	0.00	0.00	0.00	0.00	0.00	0.00	0.00	0.00
Fe	3.01	2.92	2.90	3.07	2.84	3.07	3.02	2.80	2.77	2.98	3.00
Ti	0.15	0.12	0.15	0.08	0.09	0.08	0.18	0.09	0.08	0.07	0.10
Mn	0.06	0.05	0.06	0.05	0.06	0.05	0.06	0.06	0.07	0.06	0.06
Zn	0.26	0.31	0.31	0.29	0.46	0.27	0.29	0.44	0.42	0.29	0.29
TOTAL	29.37	29.33	29.29	29.45	29.36	29.48	29.36	29.34	29.33	29.45	29.39
XMg	0.13	0.12	0.13	0.12	0.11	0.12	0.12	0.11	0.11	0.12	0.13
XFe	0.87	0.88	0.87	0.88	0.89	0.88	0.88	0.89	0.89	0.88	0.87

Table 2 (cont.)

Garnets	core	core	rim	rim	core	core	rim
SiO2	37.25	37.11	37.27	37.15	37.18	37.35	37.32
MgO	1.46	1.53	1.56	1.66	1.54	1.49	1.61
Al2O3	20.89	20.65	20.91	21.16	21.05	21.24	21.06
CaO	1.87	2.02	1.69	1.53	1.75	1.7	1.47
TiO2	0.05	0.06	0.05	0.00	0.03	0.02	0.07
FeO	31.39	32.05	32.99	33.57	32.66	32.47	33.77
MnO	6.67	5.96	5.36	4.84	5.9	6.01	5.12
Total	99.58	99.38	99.83	99.91	100.11	100.28	100.42
No. Cations in Formula (on the basis of 24 O)							
Si	6.057433	6.0541	6.050029	6.024477	6.025095	6.033615	6.030285
Mg	0.35	0.37	0.38	0.4	0.37	0.36	0.39
Al	4.004203	3.970946	4.000989	4.044748	4.020888	4.044425	4.011159
Ca	0.325781	0.353046	0.293905	0.265812	0.303819	0.29421	0.254469
Ti	0.006114	0.00736	0.006103	0	0.003656	0.002429	0.008505
Fe	4.268319	4.372097	4.477994	4.552134	4.425617	4.386038	4.562789
Mn	0.91864	0.823497	0.736919	0.664757	0.809774	0.822278	0.700686
sumX2+	5.87	5.92	5.89	5.88	5.91	5.86	5.91
Total (T)	15.93435	15.95307	15.94337	15.95315	15.96081	15.94174	15.95563
End-member calculations							
PY	6.0	6.3	6.4	6.8	6.3	6.1	6.6
ALM	72.8	73.8	76.1	77.4	74.9	74.8	77.3
GRO	5.6	6.0	5.0	4.5	5.1	5.0	4.3
SP	15.7	13.9	12.5	11.3	13.7	14.0	11.9
XMg	0.1	0.1	0.1	0.1	0.1	0.1	0.1

Table 2 (cont.)

Micas	Muscovite							Biotite		
Na2O	1.03	1.21	1.30	1.11	1.20	0.76	0.95	0.14	0.15	0.13
SiO2	46.29	46.21	45.95	46.10	46.93	46.19	45.62	34.15	35.19	34.70
MgO	0.37	0.31	0.36	0.25	0.43	0.35	0.42	8.10	7.77	7.81
Al2O3	36.48	37.10	37.29	37.51	36.31	37.06	37.11	19.68	19.65	19.05
K2O	9.49	9.24	9.38	9.52	9.26	9.05	9.33	7.29	7.98	7.45
TiO2	0.20	0.27	0.24	0.31	0.31	0.28	0.13	1.48	1.68	1.92
FeO	0.96	0.66	0.70	0.75	0.91	1.14	1.01	23.19	22.77	23.01
MnO	0.00	0.02	0.01	0.01	0.00	0.00	0.00	0.08	0.07	0.09
Total	94.83	95.01	95.23	95.56	95.34	94.83	94.58	94.10	95.25	94.16
No. Cations in Formula (on the basis of 22 O)										
Na	0.265	0.310	0.333	0.283	0.306	0.195	0.245	0.042	0.045	0.039
Si	6.143	6.105	6.069	6.068	6.183	6.110	6.068	5.304	5.393	5.383
Mg	0.073	0.061	0.071	0.049	0.084	0.069	0.083	1.875	1.775	1.806
Al	5.706	5.778	5.806	5.820	5.638	5.779	5.819	3.603	3.549	3.484
K	1.606	1.557	1.580	1.598	1.556	1.527	1.583	1.444	1.560	1.474
Ti	0.020	0.027	0.024	0.031	0.031	0.028	0.013	0.173	0.194	0.224
Fe	0.107	0.073	0.077	0.083	0.100	0.126	0.112	3.012	2.918	2.985
Mn	0.000	0.002	0.001	0.001	0.000	0.000	0.000	0.011	0.009	0.012
TOTAL	13.920	13.913	13.961	13.932	13.899	13.834	13.923	15.464	15.441	15.407
XMg	0.407	0.456	0.478	0.373	0.457	0.354	0.426	0.384	0.378	0.377
Si*	3.07	3.05	3.03	3.03	3.09	3.06	3.03	2.65	2.70	2.69

* calculated based on half-formula

Table 3 – Comparative table for main characteristics of Várzea do Capivarita Complex (VCC) and Cerro da Árvore Complex (CAC)

Characteristic	VCC	Reference (method)	CAC ("Porongos I")	Reference (method)
Igneous protolith geochemistry	Arc-like, medium- to high-K calc-alkaline	Martil et al., 2011, 2017;	Arc-like, medium- to high-K calc-alkaline	Battisti et al., 2018
Magmatic age	789.7 ± 8.7 Ma 770 ± 9.9 Ma 788 ± 5.3 Ma 790 ± 34 Ma	Martil, 2016 (U-Pb zircon, LA-ICP-MS and SHRIMP)	[1] 789 ± 7 Ma [2] 789 ± 39 Ma [3] 773±3.1; 801±4.7 [3'] 809 ± 4.1 Ma [4] 773 ± 8 Ma	[1] Saalmann et al., 2011 (U-Pb zircon LA-ICP-MS) [2] Soliani Jr., 1986 [3] Pertille et al., 2017 (U-Pb zircon [2,3]SHRIMP and [3']LA-ICP-MS) [4] Chemale Jr., 2000 (U-Pb zircon TIMS)
Metasedimentary provenance	MDA: 728 ± 11 Ma 1.4; 2 – 2.2 Ba	Gruber et al., 2016a (U-Pb zircon, SHRIMP)	800 – 780 Ma 1.4; 2 – 2.2 Ba	Gruber et al., 2016b (U-Pb zircon, LA-ICP-MS)
Metamorphic age	[5] 648.4 ± 5.4 Ma 648 ± 18 Ma [6] 618 ± 7.3 Ma [7] 614 ± 12 Ma ~~652 ± 26 Ma~~ 605.9 ± 2.4 Ma [8] 619 ±4.3 Ma	[5] Martil, 2016 (U-Pb zircon SHRIMP+LA-ICP-MS) [6] Gruber et al. 2016a (U-Pb zircon SHRIMP) [7] Gross et al., 2006 (Sm-Nd garnet-whole rock isochron) [8] Philipp et al., 2016b (U-Pb zircon SHRIMP)	[9] 658 ± 26 Ma	[9] Lenz, 2006 (Rb-Sr isochron muscovite-whole- rock composite of 5 samples)
Metamorphic conditions	[10] 730 – 800°C 3 – 4 Kbar [11] 790 – 820°C/ 4.4 - 4.8 Kbar (M1) [11] 665 - 725 °C/ 2.8 - 3.4 Kbar (M2) [12] 800 °C/ 4.6 Kbar (M1) [12] 680 °C/2.8 Kbar (M2)	[10] Gross et al., 2006 (THERMOCALC several samples) [11] This work (Perple_X - VCC northern roof pendant) [12] Costa et al., 2020 (Perple_X - VCC southern roof pendant)	[14] 590 °C/6 Kbar (M1) [14] 550 °C/2.7 Kbar (M2) [15] 560 – 580 °C 5.8 - 6.3 Kbar	[14] Lenz, 2006 (THERMOCALC) [15] This work (Perple_X)
Structural pattern	NNW-striking transpress. thrust-to-W to dextral strike-slip	Martil et al., 2011 Martil, 2016, De Toni et al., 2016	NNW-striking transpress. thrust-to-W to D_2 (dextral?) strike-slip	Jost and Bitencourt, 1980 Battisti et al., 2018